THE ASTRONOMICAL JOURNAL VOLUME 110, NUMBER 3 SEPTEMBER 1995

AN X-RAY SURVEY OF THE OPEN CLUSTER NGC 6475 (M7) WITH *ROSAT*

CHARLES F. PROSSER AND JOHN R. STAUFFER
Harvard–Smithsonian Center for Astrophysics, 60 Garden Street, MS-66, Cambridge, Massachusetts 02138

J.-P. CAILLAULT
University of Georgia, Department of Physics & Astronomy, Athens, Georgia 30602

SUCHITRA BALACHANDRAN
Ohio State University, Astronomy Department, 174 West 18th Avenue, Columbus, Ohio 43210

ROBERT A. STERN
Lockheed Palo Alto Research Laboratory, O/91-30 Building 252, 3251 Hanover Street, Palo Alto, California 94304

SOFIA RANDICH
Max-Planck Institut für Extraterrestrische Physik, D-85740 Garching, Germany

Received 1995 March 10; revised 1995 April 10

ABSTRACT

A *ROSAT* x-ray survey, with complimentary optical photometry, of the open cluster NGC 6475 has enabled the detection of ~50 late-F to K0 and ~70 K/M dwarf new candidate members, providing the first reliable detection of low-mass stars in this low galactic latitude, 220 Myr old cluster. The x-ray observations reported here have a typical limiting sensitivity of $L_x \simeq 10^{29}$ erg/s. The detection frequency of early type cluster members is consistent with the hypothesis that the x-ray emitting early type stars are binary systems with an unseen, low-mass secondary producing the x rays. The ratio between x-ray and bolometric luminosity among NGC 6475 members saturates at a spectral-type/color which is intermediate between that in much younger and in much older clusters, consistent with rotational spindown of solar-type stars upon their arrival on the ZAMS. The upper envelope of x-ray luminosity as a function of spectral type is comparable to that of the Pleiades, with the observed spread in x-ray luminosity among low-mass members being likely due to the presence of binaries and relatively rapid rotators. However, the list of x-ray selected candidate members is likely biased against low-mass, slowly rotating single stars. While some preliminary spectroscopic information is given in an appendix, further spectroscopic observations of the new candidate members will aid in interpreting the coronal activity among solar-type NGC 6475 members and their relation to similar stars in older and younger open clusters. © *1995 American Astronomical Society.*

1. INTRODUCTION AND PREVIOUS WORK

NGC 6475 (M7) is a fairly populous southern open cluster [$17^h50.6^m$, $-34°48'$ (1950)] with a galactic latitude of $b \simeq -4.5°$. A recent study based on the high-mass membership yields an age of ~220 Myr and a distance of ~240 pc (Meynet *et al.* 1993). Previous investigations include the photometric studies of the brighter cluster members ($V \leq 11$) by Koelbloed (1959) and Hoag *et al.* (1961), both of which provide finding charts. Spectral types are reported by Abt (1975), who also reviews all of the main references up to that time. Snowden (1976a) provides the most comprehensive reddening and distance information for NGC 6475, including a review of all previous reddening and distance moduli estimates. Snowden finds $(m-M)_0 = 7.06$ (~260 pc), $E(B-V) = 0.096$, resulting in an apparent distance modulus of ~7.35.

Other previous work in NGC 6475 which has appeared since the review by Abt (1975) is given here for completeness. A study of the eclipsing binary cluster member Koelbloed 86 (=HD 162724) is reported by Leung & Schneider (1975). More recently, Gieseking (1985) conducted a radial velocity survey using objective prism plates, and Mermilliod *et al.* (1989) derived a 217 day, circular orbit for HD 162391, one of three red giants in NGC 6475. Six A-type members were monitored by Engberg (1983) in an attempt to detect measurable variability among normal A-type stars. Lodén (1984) carried out a spectroscopic study of about 20 B and A cluster members.

A note relating to a proper motion study of NGC 6475 is given in Constantine *et al.* (1969). No individual membership probabilities are given, though Snowden (1976a) did employ the proper motion results in his assessment of membership for the Koelbloed stars (using an unpublished version of the Constantine *et al.* study). The Constantine *et al.* proper motion survey is of limited effectiveness in segregating cluster stars from field stars due primarily to the cluster's large distance and consequently small relative motion to the field. Indeed, Constantine *et al.* note that the main source of uncertainty in their results is the small relative cluster motion.

A major goal of the present investigation is to extend the known membership of NGC 6475 beyond the mid/late-F

 0004-6256/95/110(3)/1229/19/$0.90

dwarf range ($V \simeq 11.0$) and identify G and K solar-type members or candidate members. Since coronal x-ray emission is pervasive among late-type stars in young stellar clusters, deep x-ray surveys with *ROSAT* have proven extremely useful in detecting new low-mass candidate cluster members in, e.g., IC 2391 and IC 2602 (Patten & Simon 1993; Randich *et al.* 1995). Other recent investigations of open clusters with *ROSAT* include studies of Pleiades, Praesepe, and Hyades stars (Stauffer *et al.* 1994; Randich & Schmitt 1995; Stern *et al.* 1994; Pye *et al.* 1994; Stern *et al.* 1995). NGC 6475 (~220 Myr) is intermediate in age between the Pleiades (~70 Myr) and the Hyades/Praesepe clusters (~700 Myr, Mermilliod 1981) and is therefore an excellent candidate for the study of x-ray emission from solar-type stars and the evolution of coronal activity with age. To identify new members of NGC 6475 and investigate their x-ray properties, we undertook an x-ray survey of the cluster using an ~46 ks *ROSAT* PSPC pointing.[1] The present paper reports on the new candidate cluster members and associated photometry; further spectroscopic observations of these candidates will be reported separately, though some preliminary observations are reported in an appendix.

2. CCD PHOTOMETRY

2.1 Observations and Reduction

CCD photometry of NGC 6475 was obtained by C.P. during 1993 April using the 0.9 m telescope at CTIO. A 2048^2 Tektronix CCD was used, providing a ~13×13 arcmin field of view (~0.8″/pixel, 2×2 binning) with some vignetting/coma near the corners of the CCD. *BV* photometry was obtained in the central cluster region for a 4×4 grid of overlapping CCD fields. *VI* photometry was obtained for an 8×7 grid of CCD fields, overlapping the *BV* coverage and extending farther out from the cluster center. The *BV* photometry covers approximately 0.5° sq. and the *VI* photometry covers ~1.5° sq. centered on the cluster. Relatively short exposure times (5–15 s) for the *BVI* exposures were employed to avoid saturating the brighter stars of interest ($V \sim 10$).

We used DAOPHOT (Stetson 1987), incorporated into the current version of the VISTA software package, to determine instrumental magnitudes using aperture photometry with annular sky subtraction. As the NGC 6475 photometry was obtained concurrently with *BVI* photometry in IC 2602 (Randich *et al.* 1995), the same extinction corrections and transformation equations to a standard *BV* (Johnson) and *I* (Cousins) system from the IC 2602 study were applied here. Standard stars from Landolt (1992), Schild (1983), and Stauffer (1982) were observed nightly and used to transform each night's instrumental magnitudes onto a standard BVI_C system. Standards with Kron-system $V-I$ colors were transformed to the Cousins $V-I$ system using the transformation equations of Bessell & Weis (1987). The standards were also used in determining the nightly aperture corrections applied to the photometry of the NGC 6475 fields.

2.2 Photometry of Koelbloed Stars

The high-mass membership of NGC 6475 is based on Koelbloed's (1959) photoelectric and photographic photometry survey of bright stars in the cluster region. Snowden (1976b) provides cross references to those Koelbloed (or "K") stars considered as members, along with a few additional stars not in Koelbloed's survey. The cluster main sequence as defined by the Koelbloed stars extends to ~F5 V. For all Koelbloed stars (whether considered members or not) *BVI* photometry was obtained from our CCD observations as long as they were not saturated. The CCD photometry is given in Table 1, where we list star name, BVI_C CCD photometry, the number of observations in each filter, and the original photoelectric or photographic photometry from Koelbloed (1959). A colon following an individual star name indicates that the CCD photometry is less reliable either because the star has a high count level in the nonlinear response region of the CCD ($V \leqslant 10.2$) or because the star lies near the edge of the CCD's field of view and thus vignetted.

In Fig. 1 we compare the *V*-band magnitudes of Koelbloed (1959) to the photoelectric photometry of Snowden (1976a) and the present CCD *V* magnitudes. For $V < 11$ a trend (or possibly a systematic offset) becomes evident in the photometry of Koelbloed, in the sense that the Koelbloed *V* magnitudes are slightly brighter (~0.1 mag) when compared to either that of Snowden (1976a) or the present photometry. Snowden himself hints at the slightly poorer agreement he found in his comparison to Koelbloed's *V* magnitudes. Koelbloed's (1959) reduction for photometry was fairly involved and it appears that there is a real offset in the *V* magnitudes of his brighter ($V < 11$) stars. A comparison of Koelbloed's $B-V$ colors with ours shows no similar offsets. When possible in this study, we have employed the new BVI_C photometry from Table 1, Snowden's *V* magnitudes, or Hoag *et al.*'s (1961) photoelectric photometry over Koelbloed's photometry. For K78, Snowden quotes $V = 10.27$, which is clearly discrepant from the *V* magnitudes of Koelbloed ($V_{pg} = 9.49$) and Hoag *et al.* ($V_{pe} = 9.56$); Snowden may have actually observed the nearby star K81, for which the *V* magnitudes of Koelbloed ($V_{pe} = 10.25$) and Hoag *et al.* ($V_{pe} = 10.30$) are in better agreement with that of Snowden.

3. X-RAY OBSERVATIONS

3.1 Data

Our PSPC observation of NGC 6475 consists of a single image comprised of two *ROSAT* pointings separated by approximately five months. Further information regarding the PSPC exposures is provided in Table 2. The two observations, of similar effective exposure times, were labeled "A" (exp~22 ks) and "B" (exp~25 ks) for convenience. The data were analyzed using the Post-Reduction Off-line Software (PROS) running under IRAF and were time filtered to exclude a few "bright Earth" time intervals containing higher count rates due to backscattered solar x-ray radiation from the Earth's atmosphere; the corresponding filtered ex-

[1] We note that a second PSPC pointing in NGC 6475 exists (Jeffries *et al.* 1994a,b), relatively near the pointing of this investigation. The two pointings should substantially increase knowledge of the low-mass membership in NGC 6475.

TABLE 1. Koelbloed star CCD photometry.

Star	CTIO CCD Phot. V	B−V	V−I_C	vbi	Koelbloed V	B−V	Ref
K1:	10.00	–	0.59	202	9.85	0.49	pg
K5	11.06	–	0.24	101	11.02	0.16	pg
K7	11.29	–	0.62	101	11.28	0.49	pg
K9:	10.28	–	1.06	202	10.18	1.12	pg
K10	11.41	–	0.45	101	11.41	0.32	pg
K11:	10.31	–	0.60	101	10.14	0.44	pg
K13:	9.96	–	0.41	101	9.76	0.24	pg
K15	10.64	0.54	0.63	312	10.56	0.55	pg
K16	11.10	0.48	0.60	624	11.12	0.42	pg
K20	10.60	1.27	–	110	10.49	1.28	pg
K21	11.62	0.46	0.62	422	11.56	0.42	pg
K25	10.11	0.23	–	110	9.95	0.25	pg
K32	10.22	0.33	–	110	10.14	0.31	pe
K33	10.44	0.37	0.46	431	10.35	0.43	pe
K35	11.30	0.30	0.47	523	11.28	0.28	pg
K36	10.59	0.14	0.21	844	10.53	0.12	pg
K39	10.33	0.37	–	330	10.23	0.36	pg
K41	10.81	0.46	0.54	211	10.77	0.49	pe
K43	10.42	0.66	0.74	211	10.26	0.69	pe
K44	11.36	0.54	0.63	211	11.38	0.47	pg
K46	11.04	1.00	1.07	211	10.98	0.96	pg
K49	10.63	0.45	0.54	523	10.59	0.42	pg
K50	11.11	0.50	0.59	211	11.09	0.49	pg
K52	11.59	0.30	0.38	312	11.65	0.22	pg
K53	11.49	–	0.69	101	11.57	0.41	pe
K57	10.93	0.49	0.62	312	10.89	0.50	pe
K64	10.15	1.67	–	110	9.98	1.78	pg
K66	10.46	0.48	0.57	422	10.44	0.46	pe
K67	10.66	0.43	0.56	422	10.57	0.48	pe
K69:	10.07	0.33	–	110	9.91	0.35	pg
K73	11.58	0.68	0.82	734	11.57	0.30	pg
K74:	10.20	0.40	–	220	10.15	0.38	pe
K75	10.58	0.43	0.54	312	10.59	0.48	pe
K76	10.86	0.51	0.61	211	10.81	0.51	pg
K80	10.79	0.55	0.66	211	10.78	0.56	pg
K81:	10.25	0.36	0.44	321	10.25	0.30	pe
K83	10.63	0.43	0.53	312	10.58	0.46	pe
K84	10.24	0.51	0.63	211	10.17	0.47	pg
K85:	10.12	0.28	0.52	211	9.94	0.26	pe
K87	11.38	0.54	0.65	211	11.35	0.51	pg
K93	11.27	0.54	0.65	211	11.22	0.50	pg
K94	10.61	0.43	0.54	211	10.41	0.51	pe
K95	11.25	0.40	0.50	422	11.27	0.34	pe
K97	11.23	0.54	0.78	312	11.27	0.50	pg
K98	11.13	0.35	0.46	211	11.11	0.35	pg
K99	10.09	–	0.44	101	9.98	0.39	pg
K100	10.78	0.34	0.40	422	10.75	0.35	pg
K102	11.17	0.53	0.64	422	11.11	0.57	pe
K106	11.16	0.76	0.83	211	11.07	0.78	pg
K107	10.64	0.66	0.76	422	10.54	0.74	pe
K113	10.78	0.51	0.61	211	10.73	0.49	pg
K115	11.21	0.52	0.62	211	11.21	0.48	pg
K117	10.51	0.40	0.55	211	10.35	0.40	pg
K119	10.98	0.49	0.61	211	10.96	0.47	pg
K127	11.08	0.51	0.62	312	11.06	0.50	pg
K128	10.03	–	0.39	101	9.97	0.34	pg
K129	10.17	–	0.43	202	10.17	0.28	pg

posure times are listed in Table 2. Further description of the *ROSAT* PSPC instrument is given in Pfeffermann *et al.* (1986) and Trümper (1992); the reader is also referred to the brief description in Stauffer *et al.* (1994).

Before combining the A and B observations listed in Table 2, the aspect solutions were checked by comparing the positions of those sources detected in the standard pipeline processing (SASS) common to both the A and B observations. Comparison of 30 common sources having off-axis distances of 16 arcmin or less showed that while there were no significant differences in right ascension, the B-observation declination values were systematically displaced north of the A-observation positions by an average of 13 arcsec (or 26 pixels at the PSPC scale of 0.5″/pixel). The NGC 6475-B observation was therefore shifted by −26 pixels in the *Y*-axis to bring it onto the coordinate system of NGC 6475-A. The combined A+B observation, totaling 46,642 s, is used in subsequent analysis. In Fig. 2 we show the combined A+B 46 ks exposure of NGC 6475. An approximate 50×50 arcmin region centered on the PSPC field and restricted to the hard band x-ray regime (pulse invariant, or "PI," channels 50–180, ~0.5–1.8 keV) is shown.

3.2 Source Detection

An initial list of x-ray sources was produced using the PROS DETECT package, employing a 30″ detection cell size for the central region (off-axis distance ≤20′) and a 120″ cell size for the outer region (off-axis distance ≥20′) of the PSPC field. The detection routines were run on a hard-band

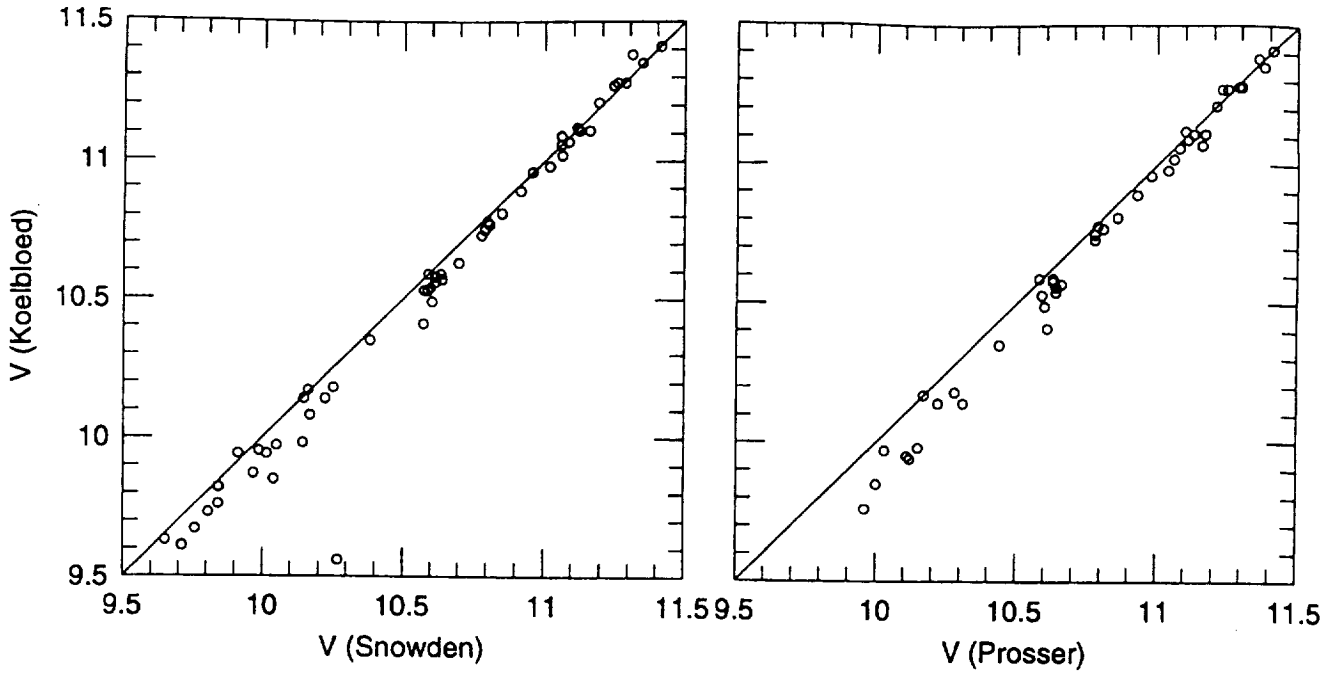

FIG. 1. Comparison of the original photometry of Koelbloed (1959) with the photoelectric V magnitudes from Snowden (1976a) and the CCD V magnitudes of this study. For $V \leq 11$, the Koelbloed magnitudes are systematically brighter (~0.1 mag). Snowden's measurement of K78 is the very discrepant point in the comparison to Koelbloed's photometry; the value for K78 quoted by Snowden may actually correspond to an observation of K81.

image (PI: 50–180) since the soft x-ray background is suppressed and the stellar x-ray spectra peak primarily in the higher-energy region because of interstellar absorption at the lower energies. We chose a threshold signal-to-noise level of 2.5 for the PROS detection analysis. (Soft-band, PI channels 10–40, and the full broadband images were additionally checked to ensure other sources were not overlooked.) The resulting PROS source lists were merged together and in a few cases, poorly determined coordinate positions were corrected upon visual inspection of the field.

Our PSPC image of the core of NGC 6475 contains more than 100 point sources with a wide range of x-ray luminosities and at least one diffuse source. In addition, given the richness and age of the cluster, there are likely to be many more cluster members within our field of view which are below our detection limit but which contribute to the apparent x-ray background in our observation. This necessarily leads to faint sources often being in the wings of bright sources and makes it difficult to adequately determine the background level for faint sources. The existing x-ray reduction packages (i.e., PROS, MIDAS) are well designed to deal with relatively uncrowded fields but are not well-equipped to detect and measure source brightnesses in heavily crowded fields. Thus, we believe that at the faint end of the x-ray luminosity function (XLF) we are likely both to miss real sources (whose fluxes and off-axis distances are such that they "should" be detected given the integration time but which are missed by PROS due to the problems noted above) and to misidentify noise peaks as true sources if we strictly adhere to some fixed S/N threshold for source detections. We have adopted the following approach to this problem, which we believe allows us to be as complete as possible without compromising the derivation of the XLF.

(1) We have made a detailed visual examination of the PSPC image, in both broad bands and hard bands, and have identified a number of sources which appear to our eye to be real but which were not found by PROS. Some of these sources when analyzed with IMCNTS (Sec. *3.3*) yield broadband S/N>2.4, and these have been retained in the main source table (i.e., Table 4) and included in all subsequent

TABLE 2. *ROSAT* PSPC observation of NGC 6475.

Name	ROSAT ID	Exp. Time	Filtered Time	Dates of Observ.
N6475-A	200983P	22,295 sec	22,295 sec	OCT. 3–7, 1992
N6475-B	200983P-1	25,198 sec	24,347 sec	MAR. 25–27, 1993

Nominal pointing position:

$(\alpha, \delta) = (17\text{h } 53\text{m } 55.2\text{s}, -34°48'36'')$ (2000) .....

$(l, b) = (355°51', -4°31')$ .....

FIG. 2. Greyscale map of the central 50′×50′ portion of the *ROSAT* observation of the open cluster NGC 6475. The scale bar indicates a distance of 10′.

analyses. Another set of our visually identified sources formally have broadband S/N<2.4 as determined by IMCNTS. We do not utilize these sources in any of the analysis or figures in the remainder of this paper. However, we provide a list of these possible sources in a separate table (i.e., Table 5) since they may provide the means to identify a few more cluster members that otherwise would be lost.

(2) In Sec. *3.4.2*, we have derived upper limits for stars that have previously been reported as members of NGC 6475 but which were not detected in our primary x-ray analysis. For a few of these stars, the IMCNTS routine returned a S/N value at or slightly above S/N=3 (broadband), however visual examination of the PSPC image suggests to us that no real source is present at these locations and we choose to consider these apparent detections as upper limits.

Figure 3 shows a contour plot of the inner PSPC field with the identified sources indicated. Inspection of Figs. 2 and 3 reveals a diffuse source of about 5′ diameter located about 10′ off-axis, centered at $[\alpha,\delta]=[17^h54^m33.8^s, -34°47'32'']$ (2000). The nature of this diffuse source will be the subject of a future investigation; a likely explanation is that it is composed of several point sources due either to a more distant, uncatalogued open cluster or a cluster of galaxies. No obvious concentration of stars or other objects is immediately apparent from visual inspection of the CCD frames of the region. While this diffuse source is not listed in our source list, a few distinct sources lying near or within the diffuse source have been identified as possibly associated with stars projected onto the more distant diffuse x-ray source.

3.3 Source Counts and Fluxes

Net broadband counts were obtained for the identified sources with the IMCNTS aperture photometry routine in PROS, using a circular source region and a concentric background annulus. Source crowding, particularly in the inner PSPC region, restricted the maximum size of the source region which could be used practically. Where necessary due to neighboring source interference, pie-shaped regions for the source and background areas were employed, and the resulting net counts corrected for the excluded pie region. In some instances the amount of source region overlap between neighboring sources was considered to be so slight and the amount of counts involved to be such a small percentage of the total source counts that the full source regions were used for both sources. Naturally this implies that photons in the overlap region were counted twice as in belonging to each source, but we consider the effect of this to be small in comparison to other influences on the net count determination, such as the uncertainties related to the background determination in crowded source regions and the corrections applied when pie slices are employed to determine net counts. Table 3 lists the source and background annulus radii

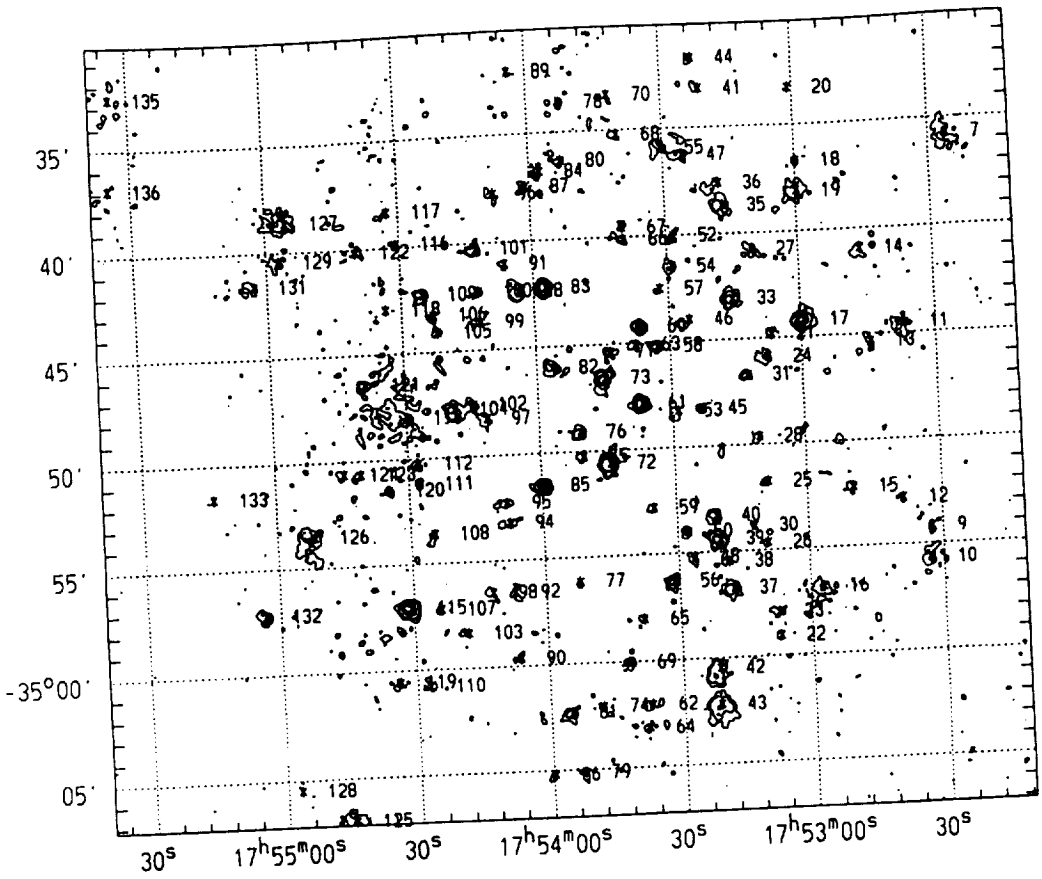

FIG. 3. Contour plot of central region of the PSPC observation of NGC 6475. As in Fig. 2, a smoothed hard band (0.5–1.8 keV) image has been used here. Sources are marked with an asterisk, followed by the x-ray source number from Tables 4 and 5.

used as a function of off-axis angle, chosen after some experimentation with various source circle sizes. As in the study of the Pleiades (Stauffer *et al.* 1994), it was necessary to mask out ≃100 of the stronger sources in the NGC 6475 x-ray image (primarily in the central 20′ PSPC region) in order that the local background measurements could be more reliably estimated. A background image with the stronger sources masked out was created and the background annulus counts were derived from this image, while the source circle counts were measured from the original, unmasked data. Since an x-ray event can only be assigned to one region in PROS, reduction of counts for multiple sources (or regions) is not practical in images with a high source density; thus, the IMCNTS task was run individually for each source to prevent errors that would occur due to overlapping source or background regions if a multisource reduction was employed. Net counts and the corresponding 1σ error in net counts were calculated with IMCNTS. The corresponding S/N for a source was calculated in the same manner as described in the analysis of the *ROSAT* x-ray observations of the Pleiades (Stauffer *et al.* 1994). As some sources, particularly the weaker ones, are more readily identified when only hard x-ray energies are considered, the net counts and corresponding S/N were calculated for each source both from the hard energy band (0.5–1.8 keV) used for source detection, and from the full broadband (0.07–2.4 keV) energy range.

TABLE 3. Source and background regions.

Off-axis Distance (arcmin)	Source (arcsec)	Background Annulus (arcsec)
≤ 10	40	70 – 120
10 – 20	80	100 – 150
20 – 35	120	150 – 250
≥ 35	200	225 – 320

The effective exposure times for each source were determined from the exposure map of the observation. To convert from counts/s to ergs/s, a 1 keV thermal source spectrum was assumed, with a hydrogen column density of $N_H = 10^{20.7}$ cm^{-2} determined using the relation between reddening and column density given in Bohlin *et al.* (1978), with reddening $E(B-V) = 0.09$. From the relations given in Fig. 10.3 of the *Rosat* Mission Description, the corresponding conversion factor is 1.25×10^{-11} ergs cm^{-2} s^{-1} per count/s.[2] This conversion factor and a cluster distance of 250 pc were then employed to convert the observed broadband count rates to x-ray luminosities.

[2]A different conversion factor will of course apply for those sources which are not associated with the cluster.

3.4 X-ray Source List and Optical Candidates

3.4.1 Source list

The x-ray source list for the NGC 6475 field is given in Tables 4 and 5, with the sources ordered by right ascension and assigned a running "R" identification number. As anticipated in Sec. *3.2*, sources with broadband S/N≥2.4 are listed in Table 4, while Table 5 contains a list of weaker possible sources with $S/N_b<2.4$. The combined Tables 4 and 5 contain a total of 141 sources and possible sources. Epoch 2000 coordinates are listed for each source along with the distance off axis from the center of the PSPC field in arcminutes. The effective exposure time is given, along with the corresponding net broadband count rate, the 1σ error in the net broadband count rate, and the signal to noise for both broadband (0.07–2.4 keV) and hardband (0.5–1.8 keV) energy ranges. The source x-ray luminosity ($\log L_x$) is given, under the assumptions discussed in the last section. A hardness ratio ("HR") has been computed as $(H-S)/(H+S)$, where H and S are the number of net counts in the hard (PI: 50–180) and soft (PI: 10–40) bands respectively. In those cases where a source was not detected in soft band, a 3σ upper limit in the soft band counts was used to give a corresponding lower limit to the hardness ratio. HR values to 0.1 accuracy are quoted only for those sources with broadband count rates greater than 0.004 counts/s, as calculation of the error in the HR value indicates 1σ errors ranging from $\sim\pm0.1$ for ~0.01 counts/s to $\sim\pm0.2$ at around 0.004–0.006 counts/s.

3.4.2 Optical counterparts

A summary of the optical counterparts identified for each x-ray source is also given in Tables 4 and 5. The *BVI* CCD photometry survey described in Sec. 2 was used to identify faint stars near the x-ray positions and bright stars in Koelbloed's (1959) survey. For a given x-ray source, several stars lying within ~30″ of the x-ray position were examined in a V vs $V-I$ and/or V vs $B-V$ color–magnitude diagram in order to ascertain whether they had photometry consistent with cluster membership (i.e., they lie between ~0.2 mag below and ~1 mag above the ZAMS). At larger off-axis distances (≥20′), offsets from the x-ray position of up to ~60″ were investigated to identify likely counterparts. In many cases, only one photometry candidate member was found near the x-ray position; if more than one such star was found, all stars were retained. Since not all x-ray sources will be associated with cluster members, we additionally considered any bright star lying near the x-ray position as a possible optical candidate for the x-ray source, even if it was a photometric nonmember of NGC 6475. The 0.8″/pixel scale of the present CCD frames at times prevented the resolution of close binaries or identification of faint, extended sources such as galaxies; in some cases later observations may reveal optical counterparts other than those presently considered.

In Tables 4 and 5 the offset in arcseconds in α and δ (x ray-optical) between x-ray and optical positions is given for each optical counterpart. This is followed by the available *BVI* photometry, the membership of the star on the basis of its photometry,[3] and the number of observations in each filter for the CTIO CCD photometry (Sec. 2). The star name [Koelbloed and/or Guide Star Catalog (GSC)] is given if available, otherwise a letter designation "A," "B," etc., is assigned. Notes are provided in the final column; weak sources which have been considered questionable upon visual inspection of the data are noted ("?source"), as are those sources which may be partially obscured by the PSPC support structure ("rib"). In the following sections we discuss some of the results of the x-ray survey of NGC 6475. Finding charts for those sources not matched to Koelbloed stars are given in Appendix A. Results of radial and rotational velocity measures for some of the optical candidates are given in Appendix B.

A. X-ray sources associated with Koelbloed stars As noted in Sec. 2.2, Koelbloed's (1959) survey of NGC 6475 provides the best membership list among early type (≤F5) stars. In Fig. 4 we show a color–magnitude diagram for those Koelbloed stars considered by us to be members of NGC 6475, indicating those stars which were detected in x rays. K45 (=R16) is considered only as a "possible" detection, since there is another photometric member located closer to the x-ray position (Table 4). The detections for K13 and K15 are uncertain due to the larger offsets and large off-axis distances involved. K69 and K70 both lie near source R59 and we cannot at this time say whether one or the other (or both) is the source of the x-ray emission. The one apparent G dwarf member, K73 (=R61), was also detected.

Among ~15 B-type members, three (~20%) are detected in x rays. For A-type members, 9 out of ~36 (~25%) are detected, and 14 out of 34 (~40%) early F dwarfs are also detected. While a comprehensive survey of binarity among early type stars in NGC 6475 is lacking, the three B-type stars detected in x rays are known single-lined spectroscopic binaries. Since normal late-type B stars are not believed to be intrinsic x-ray sources, we suspect that the observed x-ray emission arises from the unseen, lower mass companion. Two of the B-type members, K63 and K72, are classified as B9.5p with weak Ca K lines as their only peculiarity, while the third star, K104, is classified as a normal B9.5 V (Abt 1975). The reader is referred to the more extensive discussions of x-ray emissions from B- and A-type stars in the review by Pallavicini (1989) and in the recent studies by Randich & Schmitt (1995) (Praesepe), Stauffer *et al.* (1994) (Pleiades), Randich *et al.* (1995) (IC 2602), Patten & Simon (1993) (IC 2391), and Caillault *et al.* (1994) (Orion).

B. Upper limits to nondetected Koelbloed stars Upper limits in $\log L_x$ have been computed for those Koelbloed member stars in Fig. 4 which were not detected in x rays. Two HD stars, not in Koelbloed's survey, are also included.

[3]Stars in Tables 4 and 5 with photometry consistent with membership are labeled "Y" or "Y?" depending on how closely the star's location matches the apparent cluster main sequence and on whether both $B-V$ and $V-I$ colors or only one color is available. Those stars clearly lying away from the expected cluster sequence in either $B-V$ or $V-I$ and thus are nonmembers or likely nonmembers are labeled "N" or "N?," while some cases, usually involving faint ($V>15$) stars near the x-ray position, are labeled as questionable candidates, "?," due to the significant contamination from field stars in this range.

TABLE 4. X-ray source list.

ID	RA (2000)	DEC	Off-axis (arcmin)	Exp. (sec)	Cnt rate (sec^{-1})	σ(rate)	S/N_b	S/N_h	logL_X (erg/s)	HR	$\Delta\alpha$ (″)	$\Delta\delta$ (″)	V	B−V	V−I_C	mem	vbi	Name	GSC	Notes
1	17 51 35.8	−34 45 15	28.8	31964	0.005	0.001	4.6	4.2	29.67	0.7	+8	+44	13.30	–	1.18	Y?	101	A	7386.0705	
2	17 51 39.1	−35 04 38	32.2	34344	0.011	0.001	7.7	7.0	30.02	0.6	−14	−11	11.91	–	1.33	N	101	A	7386.0594	
	–	–	–	–	–	–	–	–	–	–	−19	−15	13.62	–	1.19	Y	101	B		
3	17 51 51.3	−34 53 14	25.8	35486	0.008	0.001	7.4	6.9	29.86	0.9	+8	+10	15.34	–	1.46	?	101	A		
	–	–	–	–	–	–	–	–	–	–	−18	+1	15.13	–	1.76	Y?	101	B		
4	17 51 51.6	−34 50 38	25.5	29595	0.005	0.001	4.2	3.3	29.64	0.4	−3	−27	9.96	0.24	0.41	Y?	–	K13	7386.0314	
5	17 51 52.0	−34 29 38	31.7	32403	0.015	0.001	10.2	9.5	30.15	0.6	+50	−3	12.60	–	0.67	N	101	A	7386.0333	near rib
	–	–	–	–	–	–	–	–	–	–	−10	+41	13.19	–	1.52	N	101	B	7386.0684	
6	17 51 55.4	−34 56 29	25.8	37303	0.011	0.001	10.6	8.6	30.03	0.6	+37	+13	10.64	0.54	0.63	Y	–	K15	7386.0587	
7	17 52 26.6	−34 35 48	22.3	31964	0.011	0.001	9.3	9.6	30.02	0.8	+3	−5	14.15	1.06	1.23	Y	211	A	7386.1205E	
	–	–	–	–	–	–	–	–	–	–	+7	−6	13.78	1.08	1.42	N?	211	B	7386.1205W	
8	17 52 31.8	−35 08 36	26.3	31281	0.005	0.001	3.9	4.2	29.63	≥ 0.4	+8	+21	14.13	1.76	2.03	N	211	A	7386.0589	
	–	–	–	–	–	–	–	–	–	–	−7	−48	–	–	–	–	–	B	7386.0936	
	–	–	–	–	–	–	–	–	–	–	−20	−41	13.48	1.98	2.81	N	211	C	7386.1157	
	–	–	–	–	–	–	–	–	–	–	−6	+23	14.31	1.56	1.55	?	211	D		
10	17 52 33.4	−34 55 46	18.2	37114	0.0056	0.0008	7.3	6.6	29.72	0.7	+11	+5	12.99	1.10	1.29	?	211	A		
11	17 52 37.6	−34 44 36	16.4	39466	0.0028	0.0007	4.1	4.2	29.42	–	−3	+4	14.23	1.04	1.31	Y	211	A		
12	17 52 39.4	−34 52 53	16.1	40571	0.0015	0.0006	2.4	2.0	29.15	–	−2	−6	15.68	1.56	1.84	Y?	211	A		?source
	–	–	–	–	–	–	–	–	–	–	−5	−1	16.38	–	2.08	?	101	B		
14	17 52 47.1	−34 41 00	15.9	39815	0.0022	0.0007	3.2	2.2	29.31	–	+4	−1	12.06	0.66	0.77	Y	422	A	7386.0359	
15	17 52 50.5	−34 52 17	13.8	42077	0.0019	0.0006	3.0	3.0	29.25	–	−8	−3	12.28	0.71	0.98	Y	523	A	7386.0151	
16	17 52 57.9	−34 56 57	14.4	41970	0.0061	0.0007	8.6	8.3	29.76	0.7	+2	−1	11.69	0.72	0.81	Y	312	A	7386.0794	
	–	–	–	–	–	–	–	–	–	–	−18	+0	9.36	0.35	–	Y	–	K45	7386.0883	
17	17 52 59.9	−34 44 17	12.2	42552	0.0090	0.0008	11.9	11.5	29.93	0.9	+3	+0	15.93	–	1.69	?	101	A		
18	17 53 00.4	−34 36 46	16.4	37667	0.0048	0.0007	6.4	2.6	29.65	−0.4	+0	−4	14.57	1.39	1.58	?	211	A		very soft
	–	–	–	–	–	–	–	–	–	–	−7	−4	14.94	1.53	1.89	?	211	B		
	–	–	–	–	–	–	–	–	–	–	+9	−14	14.27	1.55	2.36	N	211	C	7386.0349	
19	17 53 00.6	−34 38 11	15.3	38928	0.0050	0.0008	6.5	7.9	29.67	≥ 0.6	+3	−5	14.24	1.07	1.34	Y	312	A		
20	17 53 01.7	−34 33 20	18.8	32115	0.0020	0.0008	2.6	3.4	29.27	–	+15	+7	11.36	0.54	0.63	Y?	–	K44	7386.0692	
21	17 53 07.5	−34 44 53	10.5	43721	0.0048	0.0006	7.9	7.2	29.65	0.9	+1	−1	9.10	0.15	–	Y	–	K48	7386.0578	
22	17 53 08.0	−34 59 10	14.3	42003	0.0022	0.0007	3.3	4.2	29.32	–	−3	−1	10.63	0.45	0.54	Y?	–	K49	7386.0558	
23	17 53 08.2	−34 58 03	13.5	42207	0.0032	0.0006	5.0	5.0	29.48	–	–	–	–	–	–	–	–			
24	17 53 08.5	−34 45 57	10.0	44091	0.0019	0.0003	5.9	6.5	29.24	–	−6	−5	11.11	0.50	0.59	Y?	–	K50	7386.0789	
25	17 53 09.6	−34 51 51	9.9	43145	0.0013	0.0003	4.3	3.6	29.08	–	−3	+4	16.39	–	2.02	?	202	A		
27	17 53 11.3	−34 40 50	11.9	42573	0.0031	0.0006	4.9	5.7	29.47	–	−8	−7	12.12	0.68	0.75	Y	211	A	7386.0904	
28	17 53 11.3	−34 49 42	9.1	43862	0.0010	0.0003	3.4	3.2	28.96	–	−3	−2	9.20	0.19	–	Y?	–	K51	7386.0228	
29	17 53 13.1	−35 13 52	26.7	36169	0.006	0.001	5.1	5.6	29.73	0.9	−4	+23	13.68	–	1.07	Y	101	A		
30	17 53 13.2	−34 53 55	10.1	43170	0.0011	0.0003	4.2	2.7	29.02	–	−1	+6	14.96	1.21	1.48	Y?	312	A		?source
31	17 53 13.4	−34 46 46	8.8	43851	0.0013	0.0003	4.5	5.3	29.09	–	+2	−6	11.49	0.41	0.69	?	–	K53	7386.0200	bad B−V?
32	17 53 15.5	−35 12 04	24.8	37779	0.008	0.001	7.8	7.4	29.89	0.8	−14	+1	15.01	–	1.71	Y?	101	A		
	–	–	–	–	–	–	–	–	–	–	−21	+2	15.28	–	1.52	Y	101	B		
33	17 53 16.2	−34 43 08	9.7	44361	0.0048	0.0004	11.7	11.6	29.65	0.9	+2	−4	13.42	0.89	0.99	Y	211	A		
34	17 53 17.4	−34 24 17	25.5	34693	0.005	0.001	4.7	4.6	29.64	0.6	−9	−11	15.08	–	1.49	Y	101	A		
35	17 53 17.6	−34 38 44	12.5	42730	0.0067	0.0007	9.6	10.3	29.80	≥ 0.7	+2	−9	14.54	1.31	1.43	Y?	422	A		
36	17 53 18.4	−34 37 41	13.3	41999	0.0034	0.0007	5.3	5.3	29.50	–	+6	−8	11.75	0.60	0.70	Y	211	A	7386.0928	
37	17 53 18.4	−34 56 50	11.2	43575	0.0062	0.0007	9.4	9.0	29.76	≥ 0.6	−18	−7	15.60	1.46	1.76	Y	312	A		
38	17 53 19.3	−34 55 33	10.1	43158	0.0018	0.0003	6.3	5.7	29.24	–	−3	+2	10.93	0.49	0.62	Y	–	K57	7386.0435	
39	17 53 21.1	−34 54 29	9.1	43586	0.0062	0.0004	14.6	14.2	29.76	1.0	−2	+6	12.36	0.71	0.79	Y	312	A	7386.1725	
	–	–	–	–	–	–	–	–	–	–	−5	−11	12.19	0.69	0.81	Y	312	B	7386.0023	
40	17 53 21.8	−34 53 22	8.4	43168	0.0030	0.0003	8.7	8.6	29.44	–	+2	−4	15.59	1.40	1.92	Y	312	A		
42	17 53 22.3	−35 00 35	13.7	42297	0.0046	0.0007	6.6	7.0	29.63	0.9	+0	−4	11.83	0.63	0.75	Y	211	A	7386.0567	
43	17 53 22.3	−35 02 18	15.3	41952	0.0100	0.0008	12.6	12.8	29.97	0.8	+2	+5	12.10	0.76	0.85	Y	211	A	7386.0655	
45	17 53 23.9	−34 48 16	6.4	44267	0.0009	0.0003	3.4	3.9	28.94	–	+0	−5	14.01	1.27	1.54	Y?	211	A		
46	17 53 26.2	−34 44 03	7.5	44446	0.0016	0.0003	5.4	5.5	29.17	–	−6	+5	13.59	0.97	1.05	Y	211	A		
	–	–	–	–	–	–	–	–	–	–	−2	+3	15.43	1.53	1.68	Y?	211	B		
47	17 53 26.3	−34 36 18	13.7	42134	0.0036	0.0007	5.4	5.9	29.52	–	+5	−2	9.81	0.31	–	Y	–	K60	7386.0187	
48	17 53 27.0	−34 55 18	8.9	43485	0.0022	0.0003	7.6	7.1	29.30	–	−8	+9	14.73	1.28	1.45	Y	211	A		
49	17 53 27.6	−34 28 48	20.6	31880	0.004	0.001	3.9	2.8	29.59	0.2	+33	+5	12.37	0.69	0.78	Y	211	A	7386.0443	near rib
	–	–	–	–	–	–	–	–	–	–	+13	−1	11.72	0.93	1.07	N	211	B	7386.0197	
50	17 53 28.3	−34 54 05	7.8	43932	0.0021	0.0003	7.2	5.6	29.30	–	+0	−7	9.65	0.44	–	Y	–	K61	7386.0476	
51	17 53 29.0	−34 14 14	34.8	28418	0.005	0.001	4.1	6.1	29.65	≥ 0.6	−19	+1	12.25	–	0.89	Y	101	A	7386.0177	
	–	–	–	–	–	–	–	–	–	–	−16	+37	12.00	–	0.71	N?	101	B	7386.1148	
52	17 53 29.1	−34 40 05	10.1	43808	0.0020	0.0006	3.3	3.3	29.28	–	−2	−9	16.01	–	3.65	N	202	A		
	–	–	–	–	–	–	–	–	–	–	+4	+2	15.13	0.77	1.01	N	422	B		
	–	–	–	–	–	–	–	–	–	–	−18	−13	15.47	1.72	1.96	?	211	C		
53	17 53 29.5	−34 48 20	5.3	44996	0.0015	0.0003	5.1	4.7	29.14	–	+3	−3	13.40	0.90	1.02	Y	211	A		
54	17 53 29.6	−34 41 31	8.8	44284	0.0016	0.0003	5.3	6.1	29.18	–	+5	+0	7.56	0.00	–	Y	–	K63	7386.0537	
55	17 53 31.2	−34 35 57	13.6	42296	0.0042	0.0007	6.4	5.8	29.59	0.7	−1	+15	12.33	0.83	0.96	Y	422	A	7386.0340	
	–	–	–	–	–	–	–	–	–	–	+3	−22	11.70	0.60	0.72	Y	422	B	7386.0935	
56	17 53 31.8	−34 56 24	9.2	43604	0.0030	0.0004	8.6	8.7	29.45	–	−1	−2	10.66	0.43	0.56	Y	–	K67	7386.0832	
57	17 53 32.6	−34 42 34	7.6	45284	0.0009	0.0002	3.6	3.2	28.91	–	−6	+8	14.02	1.00	1.12	Y	422	A		?source
58	17 53 33.4	−34 45 14	5.6	45533	0.0022	0.0003	7.1	6.8	29.30	–	+4	+0	9.02	0.18	–	Y		K70	7386.0075	
	–	–	–	–	–	–	–	–	–	–	+5	−13	10.07	0.33	–	Y	–	K69	7386.0251	
59	17 53 35.9	−34 52 53	5.8	43985	0.0006	0.0003	2.4	3.3	28.76	–	+2	+1	16.74	–	2.24	?	202	A		
60	17 53 36.9	−34 44 18	5.7	44478	0.0038	0.0004	10.6	10.0	29.55	–	+1	−5	8.20	0.00	–	Y	–	K72	7386.0138	

TABLE 4. (continued)

ID	RA (2000)	DEC	Off-axis (arcmin)	Exp. (sec)	Cnt rate (sec^{-1})	σ(rate)	S/N_b	S/N_h	$\log L_X$ (erg/s)	HR	$\Delta\alpha$ (″)	$\Delta\delta$ (″)	V	B−V	V−I_C	mem	vbi	Name	GSC	Notes
61	17 53 37.4	−34 47 55	3.7	45256	0.0064	0.0004	14.4	14.3	29.77	0.9	+2	−6	11.58	0.68	0.82	Y	–	K73	7386.0255	
63	17 53 38.4	−34 45 09	4.9	44959	0.0017	0.0003	6.0	5.7	29.20	–	+1	−6	15.20	1.37	1.80	Y?	422	A		
64	17 53 38.7	−35 03 15	15.0	41884	0.0014	0.0005	2.9	2.0	29.12	–	−4	+6	11.96	0.73	0.80	Y	211	A	7386.0171	(double)
65	17 53 39.0	−34 58 08	10.1	43499	0.0019	0.0006	3.4	4.3	29.25	–	+5	+3	10.58	0.43	0.54	Y	–	K75	7386.0370	
66	17 53 40.3	−34 40 11	9.0	44946	0.0013	0.0003	4.5	5.2	29.10	–	+4	−7	12.78	0.78	0.87	Y	422	A	7386.0462	
67	17 53 40.5	−34 39 37	9.5	44330	0.0009	0.0003	3.0	3.9	28.92	–	+10	−24	15.24	–	1.86	Y?	101	A		?source
68	17 53 41.0	−34 35 16	13.7	42205	0.0037	0.0007	5.6	4.6	29.53	–	+2	−6	15.18	1.69	1.73	Y?	211	A		
70	17 53 42.7	−34 33 25	15.4	40322	0.0027	0.0006	4.2	4.1	29.41	–	+12	−3	15.31	1.40	1.55	Y	211	A		?source
	–	–	–	–	–	–	–	–	–	–	−3	+15	15.07	1.62	1.64	?	211	B		
	–	–	–	–	–	–	–	–	–	–	+18	+15	15.68	–	1.89	?	101	C		
71	17 53 44.2	−34 45 26	3.9	45366	0.0021	0.0003	7.0	7.0	29.29	–	+10	+2	14.15	1.17	1.45	Y	211	A		
72	17 53 45.0	−34 50 41	3.0	45490	0.0133	0.0006	22.8	21.9	30.09	0.9	+2	−4	10.79	0.55	0.66	Y	–	K80	7386.0778	
73	17 53 45.5	−34 46 40	2.8	45514	0.0067	0.0004	15.3	15.3	29.80	0.9	+2	−3	10.95	0.57	0.69	Y	211	A	7386.0355	
74	17 53 48.8	−35 02 10	13.6	42161	0.0036	0.0006	5.9	4.7	29.53	–	+7	−10	16.32	–	2.23	?	101	A		
	–	–	–	–	–	–	–	–	–	–	+7	+6	15.93	1.76	1.89	Y?	211	B		
75	17 53 51.1	−34 50 20	1.9	45177	0.0010	0.0003	3.6	3.2	28.95	–	+8	+2	15.57	1.95	3.44	N?	211	A		
	–	–	–	–	–	–	–	–	–	–	+3	−2	16.82	–	2.02	?	101	B		
	–	–	–	–	–	–	–	–	–	–	−3	+10	16.63	–	2.08	?	101	C		
76	17 53 51.3	−34 49 10	1.0	45714	0.0023	0.0003	7.1	7.5	29.33	–	+11	−2	13.55	0.95	1.02	Y	211	A		
77	17 53 53.0	−34 56 15	7.6	44573	0.0007	0.0003	2.6	3.5	28.82	–	+3	+1	13.85	0.74	0.88	N	211	A		
	–	–	–	–	–	–	–	–	–	–	−5	+10	13.86	2.01	2.61	N	211	B		
79	17 53 53.5	−35 05 15	16.6	40032	0.0023	0.0006	3.6	4.3	29.32	–	+5	+0	11.92	0.76	0.82	Y	211	A	7386.1293	
80	17 53 53.5	−34 36 23	12.2	42945	0.0019	0.0003	6.0	5.2	29.25	–	−1	−10	15.53	2.21	2.95	N	211	A		
	–	–	–	–	–	–	–	–	–	–	+33	−5	14.98	1.33	1.50	Y	211	B		
	–	–	–	–	–	–	–	–	–	–	−31	−7	15.86	–	1.82	Y?	101	C		
81	17 53 55.8	−35 02 24	13.8	42636	0.0028	0.0007	4.3	5.2	29.42	–	−1	+4	11.38	0.54	0.65	Y	–	K87	7386.0156	
82	17 53 57.0	−34 46 04	2.6	45629	0.0023	0.0003	7.0	7.7	29.34	–	−2	−1	12.87	0.73	0.89	Y?	211	A		
83	17 53 58.0	−34 42 16	6.4	45019	0.0066	0.0005	14.7	14.5	29.79	1.0	+1	−6	14.00	1.11	1.44	Y	211	A		
84	17 53 58.4	−34 36 51	11.8	43819	0.0020	0.0003	6.1	5.4	29.27	–	−8	+6	15.42	1.43	1.49	Y	312	A		
85	17 53 59.9	−34 51 37	3.2	46049	0.0050	0.0004	12.5	11.8	29.67	0.9	−8	−7	15.85	1.63	2.00	Y?	211	A		
86	17 54 00.3	−35 05 19	16.7	38491	0.0011	0.0003	3.5	4.5	29.01	–	−16	+3	13.68	1.13	1.24	Y	211	A		
87	17 54 01.7	−34 37 32	11.1	43768	0.0012	0.0003	4.1	3.8	29.06	–	−1	+0	15.56	–	2.16	?	101	A		
88	17 54 04.1	−34 42 24	6.5	44573	0.0042	0.0004	10.8	10.2	29.60	0.8	+1	−4	9.71	1.02	–	N	–	K91	7386.0613	
91	17 54 07.2	−34 41 05	7.9	43303	0.0018	0.0003	6.3	5.3	29.23	–	−9	+12	15.95	1.51	1.77	Y	211	A		
92	17 54 07.7	−34 56 36	8.4	44758	0.0012	0.0003	4.0	4.2	29.04	–	+1	+4	12.46	0.69	0.77	Y	211	A	7386.0986	
93	17 54 08.1	−34 29 15	19.5	27313	0.0032	0.0009	3.7	4.0	29.48	–	+9	−28	11.23	0.54	0.78	Y	–	K97	7386.0258	near rib
94	17 54 08.3	−34 53 18	5.4	44685	0.0015	0.0003	5.0	4.7	29.14	–	−15	−7	13.30	0.87	0.94	Y	211	A		
95	17 54 08.8	−34 52 21	4.7	44994	0.0015	0.0003	5.3	5.4	29.16	–	−3	−3	12.19	0.68	0.78	Y	211	A	7386.0275	
96	17 54 09.1	−34 37 47	11.2	43443	0.0024	0.0006	3.8	4.2	29.35	–	+2	+17	14.85	1.12	1.27	?	422	A		
	–	–	–	–	–	–	–	–	–	–	−1	−8	14.57	0.70	0.93	N	422	B		
	–	–	–	–	–	–	–	–	–	–	−16	+2	15.04	1.35	1.65	Y?	211	C		
97	17 54 12.6	−34 48 20	3.6	45753	0.0016	0.0003	5.4	5.1	29.18	–	−3	−2	12.17	0.69	0.76	Y	422	A	7386.0040	
98	17 54 12.8	−34 56 36	8.8	44427	0.0014	0.0003	4.6	4.3	29.10	–	−6	+5	15.23	1.74	2.14	?	211	A		
99	17 54 13.2	−34 43 47	6.1	44005	0.0018	0.0003	6.2	5.4	29.22	–	−14	−7	6.89	0.02	–	Y	–	K104	7386.0897	
100	17 54 13.3	−34 42 21	7.3	43835	0.0008	0.0003	3.0	2.5	28.90	–	−9	+2	15.75	0.83	1.11	N	211	A		
	–	–	–	–	–	–	–	–	–	–	−21	+24	15.79	–	1.87	Y?	101	B		
101	17 54 13.6	−34 40 19	9.1	43926	0.0018	0.0003	5.3	5.9	29.22	–	+2	−6	15.02	1.39	1.61	Y	211	A		
102	17 54 15.6	−34 47 38	4.3	44264	0.0021	0.0003	6.4	7.0	29.30	–	+1	−6	13.32	0.89	1.05	Y	422	A		
103	17 54 18.8	−34 58 28	11.0	43559	0.0038	0.0006	6.2	6.1	29.55	–	−4	−5	12.37	0.71	0.78	Y	211	A	7386.0850	
104	17 54 19.9	−34 47 50	5.1	44625	0.0047	0.0004	11.9	11.3	29.64	1.0	−4	−6	12.37	0.82	0.92	Y	422	A	7386.0332	
105	17 54 22.9	−34 44 10	7.2	43198	0.0013	0.0003	4.4	4.0	29.08	–	+2	−11	12.32	0.70	0.80	Y	422	A	7386.0672	
107	17 54 24.7	−34 57 17	10.6	43145	0.0017	0.0003	5.2	4.2	29.19	–	+15	+0	15.80	–	1.78	Y?	101	A		
108	17 54 25.5	−34 53 41	8.0	44192	0.0007	0.0003	2.5	2.0	28.84	–	−19	+1	12.73	0.35	0.47	N	312	A		
	–	–	–	–	–	–	–	–	–	–	+10	−15	15.82	–	1.92	Y?	101	B		
109	17 54 25.9	−34 42 22	8.9	43363	0.0020	0.0003	6.0	5.5	29.27	–	−2	−8	12.63	0.80	0.95	Y	422	A	7386.1799	
110	17 54 27.9	−35 00 54	14.0	41786	0.0016	0.0006	2.4	2.4	29.16	–	−3	+5	16.06	1.89	1.89	?	211	A		
111	17 54 28.4	−34 51 17	7.3	45176	0.0011	0.0003	4.0	4.5	29.02	–	+3	−15	13.42	0.89	0.97	Y	211	A		
	–	–	–	–	–	–	–	–	–	–	−6	−6	14.87	1.64	1.70	?	211	B		
112	17 54 28.5	−34 50 20	7.0	45002	0.0023	0.0003	7.3	7.3	29.33	–	−6	−6	16.33	–	2.10	?	101	A		
113	17 54 30.4	−34 48 08	7.2	43767	0.0042	0.0004	11.3	10.3	29.59	0.9	+1	−5	13.55	1.48	1.62	N	312	A	7386.1637	nebulous
	–	–	–	–	–	–	–	–	–	–	+3	−9	15.20	1.54	2.00	?	422	B		
	–	–	–	–	–	–	–	–	–	–	−5	−4	14.98	0.81	1.02	N	422	C		
115	17 54 31.4	−34 57 11	11.3	42605	0.0177	0.0009	19.9	11.2	30.22	−0.1	+7	−9	14.08	1.96	2.33	N	211	A		very soft
	–	–	–	–	–	–	–	–	–	–	−3	−6	15.20	1.49	2.60	N	211	B		
	–	–	–	–	–	–	–	–	–	–	−6	+6	15.43	0.98	1.20	N	211	C		
	–	–	–	–	–	–	–	–	–	–	+12	+19	14.89	1.95	2.29	N	211	D		
116	17 54 31.6	−34 39 56	11.5	42873	0.0027	0.0006	4.4	3.2	29.41	–	+5	−2	12.81	0.89	1.04	Y	211	A		
118	17 54 34.3	−34 43 00	9.8	42971	0.0010	0.0003	3.2	3.9	28.96	–	−6	+12	16.33	–	2.09	?	101	A		?source
	–	–	–	–	–	–	–	–	–	–	+18	−18	15.36	1.29	1.63	Y?	211	B		
119	17 54 34.4	−35 00 40	14.5	41053	0.0018	0.0007	2.7	2.7	29.23	–	−29	+10	12.92	0.81	0.99	Y	211	A	7386.1689	
	–	–	–	–	–	–	–	–	–	–	−12	+16	13.46	0.91	1.02	Y	211	B		
120	17 54 35.1	−34 51 33	8.7	44472	0.0010	0.0003	3.5	2.7	28.97	–	−3	−6	9.06	0.14	–	?	–	K116	7386.1429	
121	17 54 39.4	−34 46 30	9.3	43130	0.0025	0.0004	7.2	6.4	29.37	–	−9	−17	13.69	0.99	1.10	Y	211	A		nebulous
122	17 54 40.6	−34 40 14	12.5	42011	0.0019	0.0007	2.9	2.2	29.25	–	−13	−7	13.97	0.85	1.04	N	211	A		
	–	–	–	–	–	–	–	–	–	–	+0	+19	15.55	–	1.78	Y?	101	B		

TABLE 4. (continued)

ID	RA (2000)	DEC	Off-axis (arcmin)	Exp. (sec)	Cnt rate (sec^{-1})	σ(rate)	S/N_b	S/N_h	logL_X (erg/s)	HR	$\Delta\alpha$ (″)	$\Delta\delta$ (″)	V	B−V	V−I_C	mem	vbi	Name	GSC	Notes
123	17 54 41.3	−34 50 44	9.7	43480	0.0009	0.0003	3.2	3.0	28.94	–	−8	+3	13.17	0.85	0.94	Y	211	A		
	–	–	–	–	–	–	–	–	–	–	–	–	–	–	–	–	–			?source
124	17 54 45.1	−34 50 42	10.4	43105	0.0008	0.0003	2.6	3.7	28.89	–	–	–	–	–	–	–	–			
125	17 54 45.5	−35 07 07	21.2	31687	0.007	0.001	6.6	8.0	29.83	≥ 0.6	−8	−5	11.28	0.68	0.82	Y	211	A	7386.1045	
126	17 54 52.3	−34 53 38	12.7	42334	0.0063	0.0007	8.6	8.5	29.77	0.8	−13	−11	11.45	0.56	0.68	Y?	211	A	7386.1828	
127	17 54 56.1	−34 38 41	16.0	40289	0.0064	0.0008	8.5	9.3	29.78	≥ 0.7	+7	−13	11.95	0.64	0.78	Y	211	A	7386.1353	
	–	–	–	–	–	–	–	–	–	–	−19	−27	11.75	–	0.72	Y	101	B	7386.1798	
128	17 54 57.6	−35 05 36	21.3	30861	0.008	0.001	7.8	7.0	29.88	0.6	+50	−14	–	–	–	–	–	A	7386.1843	rib
129	17 54 57.9	−34 40 29	15.2	40299	0.0047	0.0007	6.8	6.5	29.64	0.9	−3	−10	14.16	1.04	1.19	Y	211	A		
130	17 55 00.0	−34 21 59	29.8	35158	0.008	0.001	7.5	8.4	29.88	1.0	+7	−16	11.46	–	1.40	N	101	A	7386.1666	
	–	–	–	–	–	–	–	–	–	–	+8	+23	15.29	–	1.75	Y?	101	B		
	–	–	–	–	–	–	–	–	–	–	+10	+32	15.65	–	1.89	Y?	101	C		
131	17 55 03.7	−34 41 39	15.7	39987	0.0035	0.0007	5.2	5.6	29.52	–	+2	+2	15.26	1.72	2.20	?	211	A		
	–	–	–	–	–	–	–	–	–	–	−17	−14	16.15	–	1.90	Y	101	B		
	–	–	–	–	–	–	–	–	–	–	+9	−15	15.65	–	1.96	Y?	101	C		
132	17 55 03.8	−34 57 18	16.5	35050	0.0049	0.0008	6.5	6.8	29.66	0.9	−4	−4	11.81	0.68	0.79	Y	211	A	7386.1351	
133	17 55 14.8	−34 51 40	16.6	35860	0.0017	0.0007	2.4	2.7	29.19	–	−9	−12	12.17	0.71	0.86	Y	312	A	7386.1920	
134	17 55 27.8	−35 26 02	41.9	29208	0.039	0.002	16.1	17.0	30.56	≥ 0.8	−60	+14	–	–	–	–	–		7386.1223	
135	17 55 35.0	−34 32 38	26.0	33757	0.008	0.001	7.2	7.2	29.88	0.8	+10	+0	13.13	–	1.14	?	101	A		
136	17 55 35.8	−34 36 55	23.7	35950	0.005	0.001	4.7	4.4	29.66	0.6	+21	+22	11.45	–	0.79	Y	101	A	7386.1707	
137	17 55 46.8	−34 42 20	23.8	37550	0.013	0.001	12.3	13.0	30.08	0.9	−1	+4	13.50	–	1.16	Y	101	A		
	–	–	–	–	–	–	–	–	–	–	−21	−44	10.31	–	0.62	Y	101	B	7386.1888	
	–	–	–	–	–	–	–	–	–	–	−23	+9	11.94	–	0.76	Y	101	C		
138	17 56 12.4	−35 02 00	31.1	34365	0.003	0.001	3.2	2.5	29.49	–	+12	−28	11.27	–	0.14	N	202	A	7386.1241	
	–	–	–	–	–	–	–	–	–	–	−33	+21	15.53	–	1.62	Y?	101	B		
139	17 56 12.6	−35 05 53	33.0	33901	0.003	0.001	3.0	3.0	29.45	–	+1	−24	15.58	–	1.99	?	101	A		
	–	–	–	–	–	–	–	–	–	–	−2	+11	15.72	–	1.78	Y?	101	B		
	–	–	–	–	–	–	–	–	–	–	−27	+9	14.87	–	1.57	Y?	101	C		
140	17 56 14.6	−34 32 40	32.8	33958	0.004	0.001	3.3	2.9	29.52	–	+58	+1	12.97	–	0.93	Y	101	A		
	–	–	–	–	–	–	–	–	–	–	−52	−41	12.38	–	0.85	Y	101	B		

The upper limit in log L_x was calculated at the 3σ level using the standard deviation in the net counts at the star's location. Following the star name, we list in Table 6 the available $(V, B-V)$ photometry, observed spectral type, off-axis distance in the PSPC field, effective exposure time, net count rate, and the associated 1σ error. The corresponding 3σ upper limit in log L_x is given, along with additional notes. Due to contamination by strong nearby sources, very stringent or reliable upper limits could not be determined for K58, K59, K76, and HD 162678. K113 and K115 lie within part of the nebulous feature (Sec. *3.2*) and it is uncertain whether they have been detected or whether the high net counts are instead due to the extended nebulous feature.

In addition to K113 and K115, there are other stars in Table 6 for which the formal broadband S/N is greater than 3, suggesting that a real X-ray source is present. In such cases the star is considered to be a detection and noted in Table 6. As they were not detected by the PROS routines and

TABLE 5. X-ray source list: Weaker possible sources.

ID	RA (2000)	DEC	Off-axis (arcmin)	Exp. (sec)	Cnt rate (sec^{-1})	σ(rate)	S/N_b	S/N_h	logL_X (erg/s)	HR	$\Delta\alpha$ (″)	$\Delta\delta$ (″)	V	B−V	V−I_C	mem	vbi	Name	GSC	Notes
9	17 52 33.2	−34 54 16	17.7	38661	0.0013	0.0007	1.9	2.6	29.09	–	−1	−14	15.50	1.40	1.49	N?	211	A		
13	17 52 45.4	−34 45 25	14.7	40997	0.0010	0.0007	1.5	1.9	28.98	–	+4	+22	9.76	0.27	–	Y	–	K38	7386.0810	
26	17 53 10.2	−34 54 44	11.1	42909	0.0004	0.0003	1.4	2.0	28.54	–	−6	−14	14.89	1.50	1.68	Y?	312	A		
	–	–	–	–	–	–	–	–	–	–	+15	−8	15.21	1.82	1.77	?	312	B		
41	17 53 22.0	−34 33 14	16.8	37160	0.0013	0.0007	1.8	1.8	29.07	–	−2	−4	15.46	1.93	1.78	Y	211	A		
	–	–	–	–	–	–	–	–	–	–	−5	+13	15.29	1.56	1.67	Y?	211	B		
	–	–	–	–	–	–	–	–	–	–	+1	+13	15.28	1.49	1.51	Y?	211	C		
44	17 53 23.6	−34 31 48	18.0	35531	0.0009	0.0007	1.2	2.2	28.92	–	+7	+8	15.44	1.52	2.94	?	211	A		
	–	–	–	–	–	–	–	–	–	–	+0	+15	14.26	1.48	1.50	?	211	B		
62	17 53 37.9	−35 02 10	14.0	42425	0.0012	0.0006	2.1	2.4	29.05	–	−2	−6	16.14	1.48	1.64	?	312	A		
69	17 53 42.3	−35 00 09	11.8	43659	0.0006	0.0006	1.0	0.8	28.77	–	−2	−2	12.13	0.66	0.80	Y	211	A	7386.0731	
78	17 53 53.4	−34 33 41	14.9	41873	0.0014	0.0007	2.2	1.1	29.13	–	−14	+2	15.51	1.25	1.63	Y?	211	A		
89	17 54 04.9	−34 32 10	16.6	39910	0.0009	0.0007	1.4	1.1	28.93	–	−8	−5	11.27	0.54	0.65	Y	–	K93	7386.0980	?source
90	17 54 07.1	−34 59 45	11.4	43262	0.0010	0.0006	1.7	3.1	28.98	–	−9	+2	12.26	0.35	0.42	N	422	A		
106	17 54 23.8	−34 43 21	7.9	43439	0.0006	0.0003	2.0	1.0	28.71	–	−7	−21	16.41	–	2.36	?	101	A		
	–	–	–	–	–	–	–	–	–	–	−14	−4	16.55	–	2.11	?	101	B		
	–	–	–	–	–	–	–	–	–	–	+8	+0	16.40	–	1.87	?	101	C		
114	17 54 30.9	−34 20 29	29.1	35201	0.0008	0.0009	0.9	1.3	28.89	–	+41	+49	11.98	–	0.86	Y	101	A	7386.1132	
117	17 54 33.2	−34 38 25	12.8	42191	0.0012	0.0006	1.9	1.7	29.06	–	+10	+2	15.90	–	1.72	Y?	202	A		
141	17 56 34.7	−34 40 35	33.7	33770	0.0012	0.0009	1.2	1.4	29.03	–	−40	−13	10.97	–	0.58	Y	101	A	7386.1243	
	–	–	–	–	–	–	–	–	–	–	−6	−9	15.54	–	1.87	Y?	101	B		

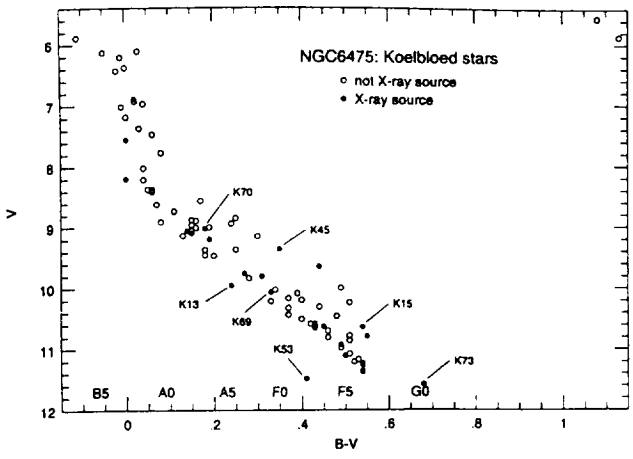

FIG. 4. V vs $B-V$ diagram for Koelbloed members are likely members of NGC 6475. Those K stars associated with x-ray sources (Table 4) are indicated; the three B-type stars detected in x rays are known binary systems. The one Koelbloed G dwarf detected in x rays is identified, along with those Koelbloed stars for which there is some uncertainty in regards to their identification as x-ray sources (see the text). The photographic $B-V$ value for K53 is likely incorrect and the star should lie along the cluster sequence. Approximate corresponding spectral types are indicated.

original visual inspection of the image, confirmation of the possible detect cases in Table 6 may need to await the results of the x-ray observation of Jeffries *et al.* Spectroscopic observation to determine the likelihood of detectable x-ray emission from the star in question would also be helpful. In the present study we treat the $\log L_x$ values for the possible detect stars as upper limits.

Neither of the two giant systems, HD 162391 or K58, was detected in our x-ray observations. Both are binary systems: HD 162391 exhibiting a 217 day orbital period and K58 being a visual binary (sep$\sim$0.4″) containing two giants, one of which is a spectroscopic binary (Mermilliod *et al.* 1989). The crowded source field near K58 prevented a very stringent or reliable upper limit from being determined for this interesting system, while HD 162391 lies fairly far off axis and has its effective exposure time reduced by rib effects. The upper limit of $\log L_x \leq 29.5$ for HD 162391 is consistent with the results for giants in the 600–800 Myr old Hyades and Praesepe clusters. All four Hyades giants have been detected in x rays with $28.3 \leq \log L_x \leq 30.0$ (see Stern *et al.* 1995), while two of the four Praesepe giants were detected at a similar level ($\log L_x = 29.8$–29.9); the remaining two Praesepe giants having upper limits of $\log L_x \leq 28.2$ (Randich & Schmitt 1995). However, the long-term variability in x-ray luminosity for giant systems is poorly understood at present (e.g., Stern *et al.* 1992), and observations of NGC 6475 at a different epoch may find detectable levels of x-ray emission from these systems.

C. New candidate members The purpose of the *ROSAT* observations in NGC 6475 was primarily to identify G and K dwarf cluster members, thus extending the membership information and providing further means of studying the evolutionary properties of solar-type stars. Indeed, in addition to the brighter Koelbloed stars detected, many fainter stars with photometry compatible with cluster membership are found to be associated with x-ray sources in the cluster region. In Figs. 5 and 6, all possible or probable members from Table 4 are plotted in V vs $B-V$ and V vs $V-I_C$ color–magnitude diagrams. Likely members from the list of Koelbloed are also plotted, along with a ZAMS shifted to the assumed distance and reddening of this $\sim$220 Myr cluster. A total of $\sim$50 new candidate members in the late-F to K0 range have been identified, along with another $\sim$70 candidate K/M dwarf members.

To assess the level of field star contamination within the group of x-ray selected candidates with photometry compatible with cluster membership, we reduced for photometry 11 CCD fields covering $\sim$0.36° sq. within the central portion of NGC 6475 and also lying within the inner PSPC region of the x-ray observation, where most x-ray candidates were found. Figure 7 shows the distribution in $(V, V-I_C)$ of the resulting general field star sample, along with those x-ray candidates from Fig. 6 which also are contained in the same area. The level of field star contamination can be found as a function of V magnitude by identifying those field stars which lie along the ZAMS ($\sim$0.2 mag below, $\sim$1.0 mag above) in Fig. 7 and computing the chance alignment with a given x-ray source within the typical ±30″ area searched for optical counterparts. The number of chance alignments will be the corresponding number of x-ray candidates contained within the same area as the field star sample, times the fraction of field stars falling within a given ±30″ region. When this is done as a function of V magnitude and adjusted to the total area of the inner PSPC field where most candidates are found, the following field star contamination levels in the x-ray selected sample are found: $\sim$4% ($\sim$3 stars out of about 70) for $10 \leq V < 14$, $\sim$10% ($\sim$2 stars out of 18) for $14 \leq V < 15$, and $\sim$40% ($\sim$15 stars out of 36) for $15 \leq V < 16$. The x-ray-selected, photometric candidates clearly reveal the cluster sequence to at least $V \sim 13.5$ (i.e., the late-G dwarfs) with the increasing contamination by field stars making the identification of cluster members for $V > 14$ more difficult until further observations can be obtained.

D. Special cases Among the sources in Table 4 are two predominantly soft x-ray sources: R18 and R115. No apparent cluster members are found from the CCD photometry at these x-ray positions. These very soft x-ray sources could be associated with foreground active stars or perhaps with a more unusual stellar system. A comparison of the CTIO CCD frames and UK Schmidt plate material does not reveal the presence of any high proper motion stars—which would presumably be nearby stars for which the soft x-ray flux has not been significantly attenuated—at the locations of R18 and R115. For both sources, several stars near the x-ray position are listed in Table 4, though none of these are extremely red or blue in color. The strongest x-ray source (R134) lies relatively far off-axis; the corresponding optical counterpart for this source has not been identified.

3.5 Cluster X-Ray Properties

We briefly discuss here some of the x-ray properties of NGC 6475; more extensive discussion awaits the acquisition of spectra of the new candidate members in order to confirm

TABLE 6. X-ray upper limits.

Star	V	B−V	Spt	Bin?	Off-axis (arcmin)	Exp. (sec)	Cnt rate (sec^{-1})	σ(rate)	$\log L_X$ (erg/s)	$3\sigma \log L_X$ (erg/s)	Notes
HD162391	5.87	1.13	K0III	SB	30.7	27426	≤0.004	–	–	≤29.52	rib
HD162678	6.38	0.00	B9V	–	2.5	45352	–	–	–	–	crowded field
K 1	10.00	0.49	–	–	37.7	32165	≤0.006	–	–	≤29.76	
K 4	8.94	0.24	A7V	–	34.2	34007	≤0.003	–	–	≤29.46	
K 6	8.96	0.15	A0IV	–	33.4	33611	≤0.004	–	–	≤29.52	
K 8	10.59	0.42	–	–	29.7	35757	≤0.003	–	–	≤29.45	
K 11	10.31	0.44	–	–	29.8	35495	≤0.003	–	–	≤29.49	
K 12	8.62	0.07	A2:	–	30.1	35176	0.003	0.001	29.50	≤29.46	poss. detect?
K 18	8.73	0.11	A1	–	23.6	36163	0.003	0.001	29.52	≤29.44	poss. detect?
K 19	9.00	0.19	A0:	–	24.1	33107	≤0.003	–	–	≤29.48	
K 23	8.88	0.15	A5	–	22.2	27923	≤0.004	–	–	≤29.52	rib
K 24	8.37	0.06	A0	–	24.4	37606	0.007	0.001	29.78	≤29.47	poss. detect?
K 26	5.89	−0.11	B5IV	–	20.9	26200	≤0.003	–	–	≤29.52	rib
K 27	9.15	0.30	F0	–	22.5	31041	≤0.003	–	–	≤29.50	near rib
K 28	8.91	0.08	A0V	–	22.8	31390	≤0.003	–	–	≤29.50	rib
K 29	8.02	0.04	A0V	–	21.9	26922	≤0.004	–	–	≤29.56	rib
K 32	10.22	0.33	–	–	22.7	24721	≤0.004	–	–	≤29.54	rib
K 33	10.44	0.37	–	–	15.3	40903	≤0.002	–	–	≤29.27	
K 34	8.21	0.04	A1V	–	16.8	39152	≤0.002	–	–	≤29.30	
K 37	9.37	0.18	–	–	22.9	23285	≤0.004	–	–	≤29.57	rib
K 39	10.33	0.37	–	–	17.2	35548	≤0.002	–	–	≤29.32	
K 40	8.85	0.25	A7V	–	18.1	32384	≤0.002	–	–	≤29.32	rib
K 41	10.81	0.46	–	–	12.6	42660	0.0031	0.0006	29.46	≤29.25	poss. detect?
K 42	6.21	−0.01	B9V	SB1	17.5	40521	≤0.002	–	–	≤29.29	
K 47	8.89	0.16	A2V	–	10.8	43863	≤0.0009	–	–	≤28.93	
K 54	10.70	0.46	–	–	11.0	42868	≤0.0009	–	–	≤28.94	
K 55	6.97	0.04	B9.5p	var?	13.9	42264	≤0.0019	–	–	≤29.25	
K 56	6.13	−0.05	B8V	–	8.7	43838	≤0.0009	–	–	≤28.91	
K 58	5.56	1.08	K0III	SB	8.3	43231	–	–	–	–	crowded field
K 59	7.19	0.00	B9.5p	SB1	14.0	41668	–	–	–	–	crowded field
K 65	9.06	0.15	A2V	–	5.9	44746	≤0.0008	–	–	≤28.89	
K 66	10.46	0.48	–	–	5.0	45185	≤0.0009	–	–	≤28.94	
K 71	7.37	0.03	B9.5V	–	5.3	44279	≤0.0008	–	–	≤28.85	
K 74	10.20	0.40	–	–	3.7	45683	0.0014	0.0003	29.13	≤28.92	poss. detect?
K 76	10.86	0.51	–	–	3.3	45437	–	–	–	–	crowded field
K 79	9.01	0.16	A2V	–	3.5	45437	≤0.0009	–	–	≤28.93	
K 82	7.77	0.08	A1V	var?	2.8	46025	≤0.0008	–	–	≤28.87	
K 83	10.63	0.43	–	–	11.9	43881	≤0.0018	–	–	≤29.24	
K 84	10.24	0.51	–	–	20.5	25383	≤0.003	–	–	≤29.40	rib
K 86	5.96	−0.01	B9V	ecl.	3.4	45441	≤0.0008	–	–	≤28.88	
K 88	6.43	−0.02	A0p	–	1.4	45343	≤0.0008	–	–	≤28.86	
K 89	8.56	0.17	A0V	–	18.0	33251	≤0.002	–	–	≤29.35	
K 92	8.41	0.06	A1V	SB1	4.8	44806	≤0.0008	–	–	≤28.87	
K 94	10.61	0.43	–	–	15.0	41585	≤0.002	–	–	≤29.28	
K 96	8.74	0.11	A1V	–	3.7	44736	≤0.0008	–	–	≤28.85	
K 99	10.09	0.39	–	–	15.2	41132	≤0.002	–	–	≤29.24	
K101	9.14	0.13	–	–	3.3	45753	≤0.0009	–	–	≤28.92	
K102	11.17	0.53	–	–	10.6	42907	≤0.0009	–	–	≤28.92	
K103	7.47	0.06	B9.5V	–	3.7	45538	≤0.0009	–	–	≤28.91	
K105	9.47	0.20	–	–	4.4	45442	≤0.0008	–	–	≤28.84	
K108	7.02	−0.01	B9V	–	6.9	43974	≤0.0008	–	–	≤28.89	
K110	6.11	0.03	Am	–	21.6	23882	≤0.004	–	–	≤29.57	rib
K113	10.78	0.51	–	–	8.3	43384	0.0011	0.0003	28.99	≤28.97	nebulous,poss. detect?
K114	9.46	0.18	–	–	8.7	43384	≤0.0010	–	–	≤28.97	
K115	11.21	0.52	–	–	8.6	43188	0.0021	0.0004	29.29	≤29.00	nebulous,poss. detect?
K117	10.51	0.40	–	–	17.1	40659	≤0.002	–	–	≤29.29	
K119	10.98	0.49	–	–	11.7	42812	≤0.002	–	–	≤29.27	
K120	10.17	0.37	–	–	14.0	41957	0.0030	0.0007	29.45	≤29.27	poss. detect?
K121	6.93	0.02	B9.5V	–	19.4	28784	≤0.002	–	–	≤29.32	near rib
K122	9.84	0.28	–	–	15.0	40016	0.0020	0.0006	29.28	≤29.28	poss. detect?
K124	8.37	0.05	A0V	–	12.3	42280	≤0.002	–	–	≤29.26	
K125	9.37	0.25	–	–	17.1	34163	≤0.002	–	–	≤29.28	rib
K127	11.08	0.51	–	–	15.9	39704	≤0.002	–	–	≤29.27	
K128	10.03	0.34	–	–	18.6	33387	≤0.002	–	–	≤29.29	rib

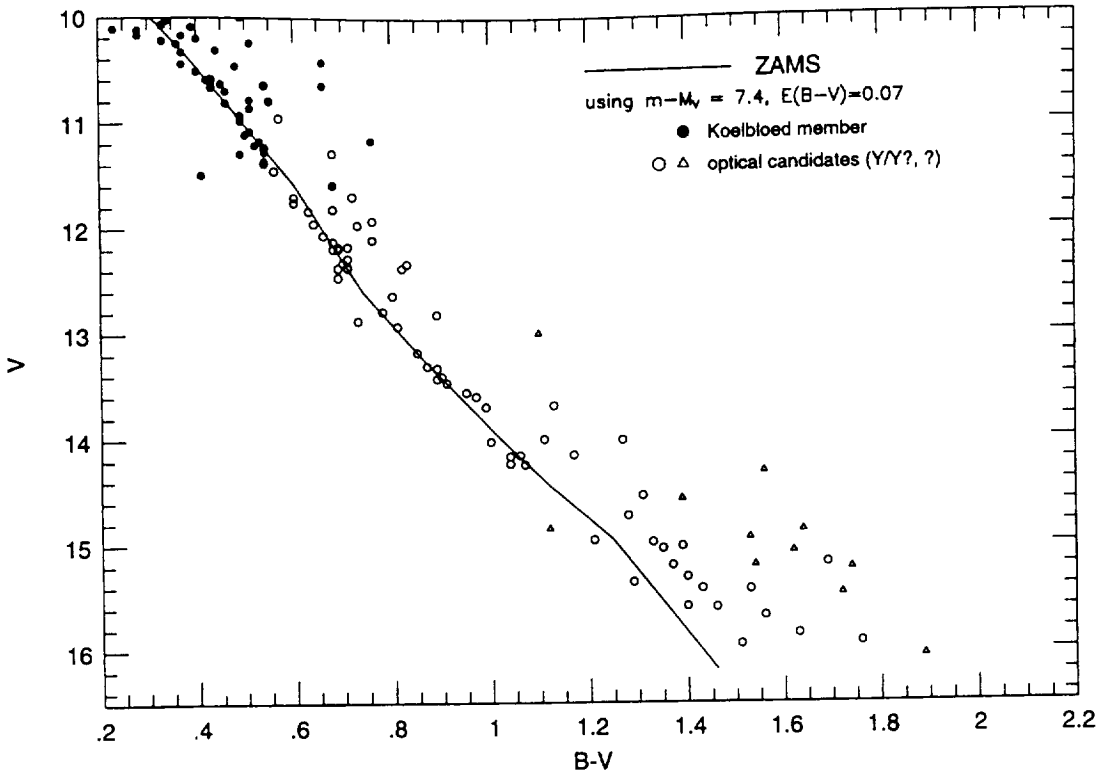

FIG. 5. V vs $B-V$ diagram of the new candidate members of NGC 6475 identified in x rays. Members and candidate members (Y/Y? candidates) from Table 4 are plotted as open circles, while uncertain (?) photometric candidates are plotted as triangles. The brighter Koelbloed members are shown for comparison. The ZAMS is from Swenson *et al.* (1994).

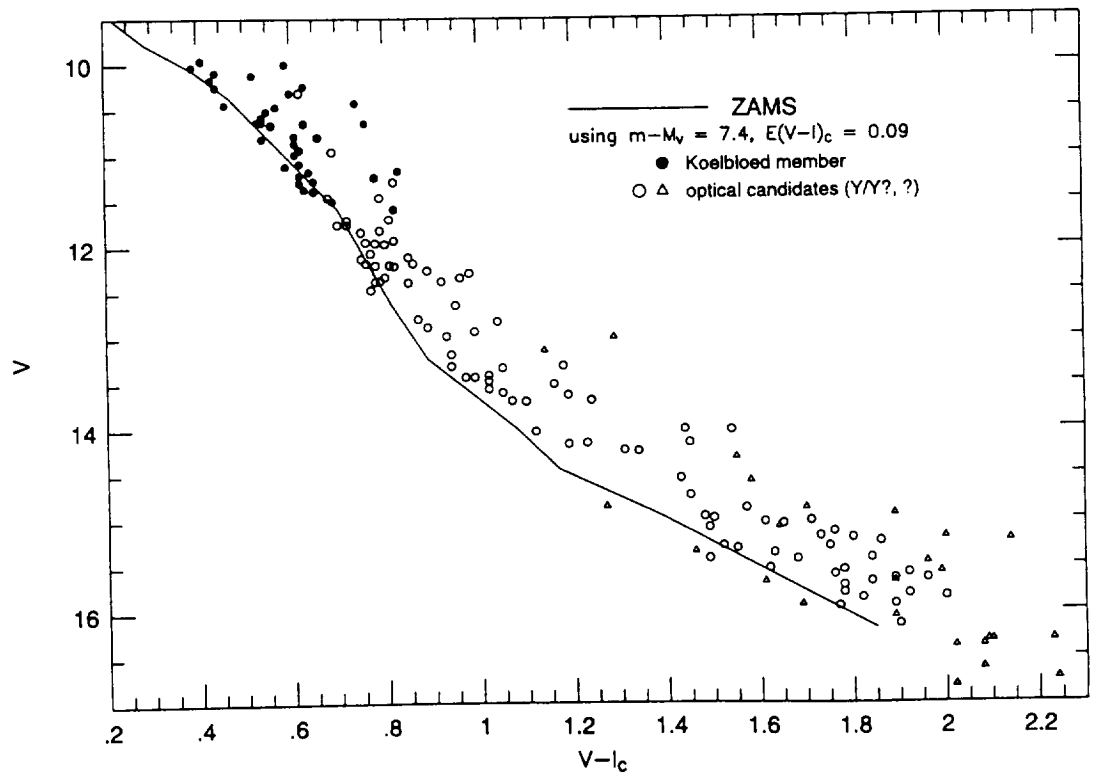

FIG. 6. Same as Fig. 5, except for V vs $V-I_C$.

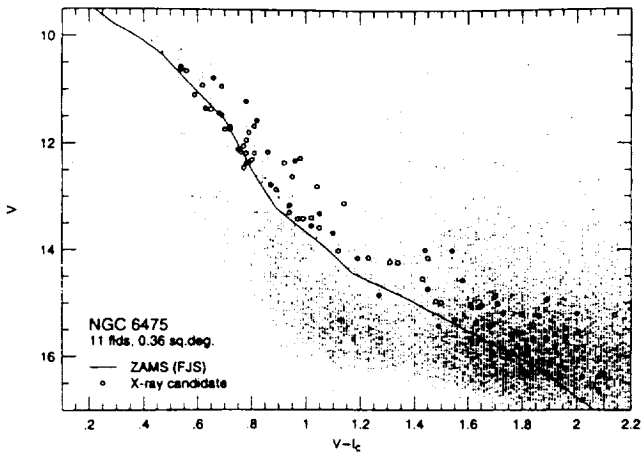

FIG. 7. Overall distribution of field stars in $(V, V-I)$ over a ~0.36° sq. area in the central cluster region used to illustrate the level of field star contamination among the x-ray selected candidates. Those candidate members selected by x rays (Table 4) lying within the same region are also indicated. The level of field star contamination is relatively low for $V<14$, though increases substantially for $V \geq 14$.

membership, detect binaries, and determine rotational velocities. Additional spectral and time-variability analysis of the x-ray sources in NGC 6475 will be discussed elsewhere. In the discussion that follows, we consider only those sources with broadband S/N≥2.4 associated with Y/Y?/? photometric candidates from Table 4.

The distribution of log L_x as a function of reddening corrected $B-V$ is shown in Fig. 8 for the cluster members and candidate members of Table 4. Upper limits in log L_x are also plotted from Table 6. The distribution of upper limits roughly falls into two categories: (a) those with log $L_x<29.0$ and off-axis distances $<11'$, and (b) those with less sensitive upper limits of log $L_x>29.0$ and off-axis distances $>11'$. We note that there are no upper limits for $B-V_0>0.5$ (other than the K0 giant HD 162391) because there is no complete faint membership list for the cluster. Using the relation between Kron and Cousins $V-I$ color from Bessell & Weis (1987) and a $B-V$ vs. $V-I_K$ relation derived from the field star photometry of Kron *et al.* (1957), approximate $B-V$ colors were estimated from $V-I_C$ colors for stars without measured $B-V$ in Table 4. There is a fair spread in log L_x as one might expect from a mixture of binary and single stars, rapid and slow rotators, and some nonmember field stars. The upper envelope in log L_x as a function of $B-V_0$ seen in NGC 6475 is similar to that seen in the Pleiades (e.g., Fig. 12, Stauffer *et al.* 1994).

In Table 7 we compare the mean and median log L_x between Pleiades and NGC 6475 stars using the same color ranges from Stauffer *et al.* (1994). The Pleiades sample has been restricted to those stars with off-axis distances within 25 arcmin as most of the NGC 6475 sources are contained within a similar central region of the PSPC field. The median and mean x-ray luminosities in each color interval have been calculated using ASURV Rev. 1.2 (LaValley *et al.* 1992), which implements the methods presented in Feigelson & Nelson (1985). For each cluster the median and mean log L_x values, error in the mean, total number of stars (N), and

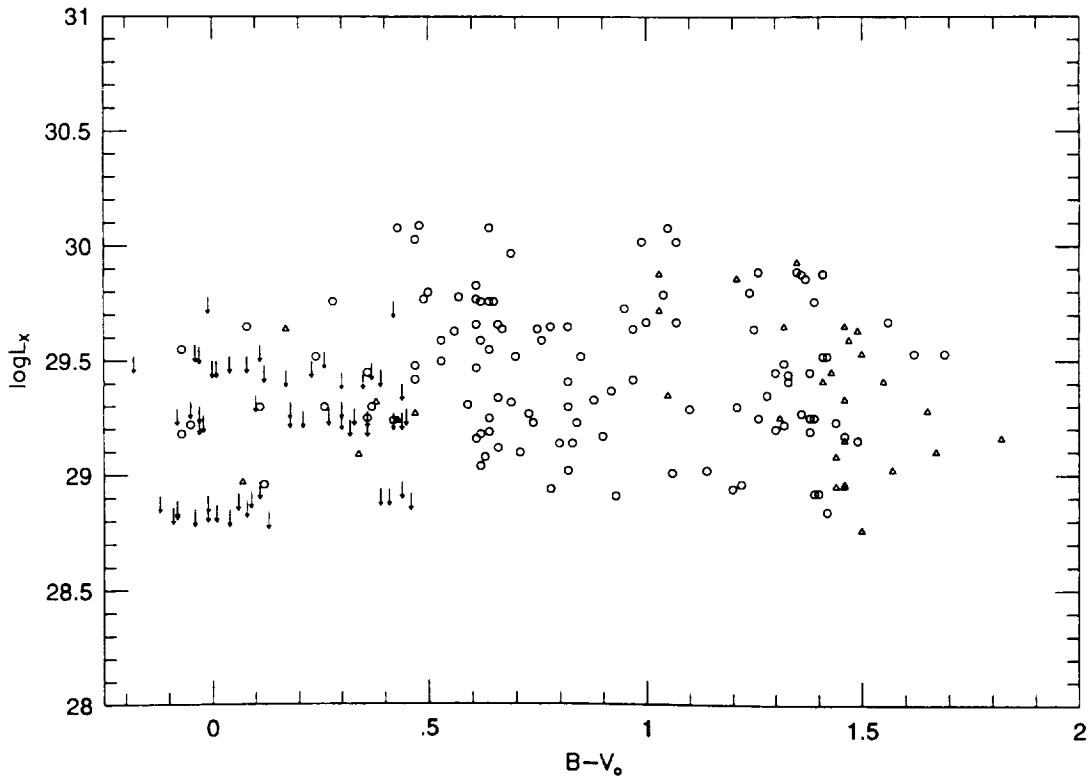

FIG. 8. Distribution of log L_x as a function of $B-V_0$ for NGC 6475. Members and candidate members (Y/Y? candidates) from Table 4 are plotted as open circles, uncertain (?) photometric candidates are plotted as triangles, and upper limits from Table 6 are indicated as downward arrows.

TABLE 7. Median and mean x-ray luminosity.

		Pleiades (off-axis < 25')			NGC 6475		
$B-V_0$	Spt	median $\log L_X$	mean $\log L_X$	N/U	median $\log L_X$	mean $\log L_X$	N/U
< 0.35	<F2	28.32[a]	28.77 ±0.11	30/17	28.84[a]	28.99 ±0.04	58/46
0.35–0.55	F2-F9	29.49	29.44 ±0.08	12/0	29.25	29.32 ±0.07	29/13
0.55–0.85	G0-G9	29.39	29.61 ±0.11	20/0	29.44	29.45 ±0.05	41/0
0.85–1.10	K0-K4	29.39	29.45 ±0.09	11/0	29.64	29.57 ±0.08	18/0
1.10–1.35	K5-K7	29.20	29.23 ±0.08	16/1	29.33	29.39 ±0.06	19/0

[a]lowest detection or upper limit.

number of upper limits (U) are given for each color interval. As seen from Fig. 8, upper limits among NGC 6475 candidates are encountered only in the first two color intervals given in Table 7. For $B-V_0<0.35$, we have listed the value of the lowest detection or upper limit in place of the median $\log L_x$, due to the large number of upper limits encountered among the B- and A-type stars.

Approximately 20 instances of x-ray sources having multiple optical candidates (i.e., Table 4) are included in the NGC 6475 tabulation; of these, almost half involve one optical candidate with $B-V_0>1.35$ and thus only the one remaining candidate is used in Table 7. In the remaining instances where multiple optical counterparts correspond to a single x-ray source, the full $\log L_x$ value was assigned to each optical counterpart. The two clusters show a fairly similar mean luminosity as a function of color until $B-V_0$ exceeds 0.85 at which point the mean Pleiades luminosity begins to dip below NGC 6475. This is probably a result of an incomplete membership list for NGC 6475 among the fainter stars, as might be derived from a proper motion analysis as was done for the Pleiades. Contamination by field stars in the NGC 6475 sample by the inclusion of the sources with multiple optical candidates does not appear to be significant; a calculation of the mean/medians for the NGC 6475 sample with the multiple optical candidates excluded finds no significant difference from those values given in Table 7.

In Fig. 9 we plot $\log(L_x/L_{bol})$ vs $B-V_0$ for the members and candidate members from Table 4. The saturation level of $L_x/L_{bol}=10^{-3}$ is apparent (see, e.g., Fleming *et al.* 1993), as is also seen in IC 2602 (Randich *et al.* 1995) and the Pleiades (Stauffer *et al.* 1994). For the early type stars ($B-V_0\leq 0.4$) the $\log(L_x/L_{bol})$ values are meaningless if one believes that the observed x-ray flux is from a late-type companion. As discussed by Randich *et al.*, lower L_x/L_{bol} levels among F/early G dwarfs are possibly the result of thinner convective envelopes in these stars, which do not support the generation of magnetic fields through dynamo activity as efficiently as the thicker convective envelopes of later-type stars. The $\sim 10^{-3}$ saturation level in $\log(L_x/L_{bol})$ appears to be reached around $B-V_0\sim 1$ for NGC 6475, compared to as early as $B-V_0\sim 0.65$ in IC 2602 (Randich *et al.* 1995), and $B-V_0\sim 1.4$ in Praesepe (Randich & Schmitt 1995) and the Hyades (Stern *et al.* 1995). This is perhaps a reflection of the evolution of low-mass stars as they spin-down over time after their arrival on the main sequence, and particularly of the fact that stars of different masses have different spin-down time scales. As these stars spin down, the level of dynamo-related coronal activity decreases, along with the level of x-ray flux.

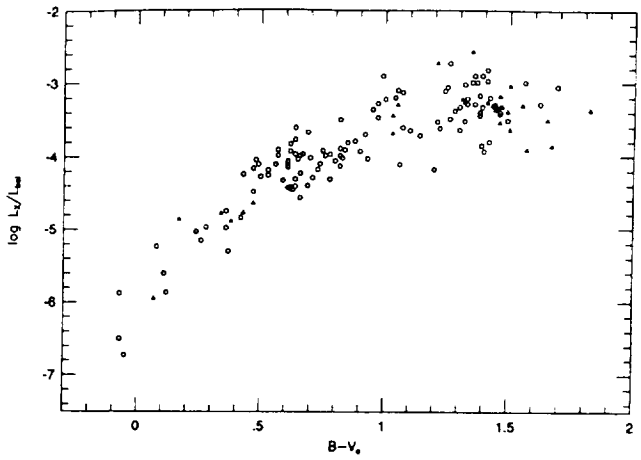

FIG. 9. $\text{Log}(L_x/L_{bol})$ vs $B-V_0$ for NGC 6475 members and candidate members from Table 4, with the same symbols used as in Fig. 8. The increasing contribution of x-ray luminosity is apparent, approaching saturation ($L_x/L_{bol}\simeq 10^{-3}$) for the latest type stars. A comparison to the older Praesepe cluster and younger IC 2602 cluster is discussed in the text.

It is this influence of rotational evolution and age on coronal activity which should be kept in mind when interpreting the observed x-ray emission in NGC 6475. For the Pleiades (age ~70 Myr), Stauffer *et al.* argued that since all known low-mass cluster members within the central PSPC regions had detectable levels of emission, the actual rotational velocities of Pleiades members were unlikely to fall much below the observed spectroscopic limit of $v \sin i\simeq 7$ km/s—a much lower rotation rate would imply a lower x-ray emission level at which stars were not detected. A comparison of $\log(L_x/L_{bol})$ vs $v \sin i$ among Pleiades stars established the existence of a rotational dependence; solar-type stars with $v \sin i\geq 10-15$ km/s exhibit an increased x-ray emission level, near or at the saturation limit. Unfortunately, unlike in the Pleiades, we have no prior low-mass membership list to guide us in NGC 6475. At the age of NGC 6475 (~220 Myr), the rotational spindown among G and K dwarfs should result in some fraction of stars having $v \sin i\leq 10$ km/s and x-ray emission below the detection sensitivity limit of $\log L_x\simeq 29.0$ in Fig. 8. This implies that we are likely to miss some (or many) slow rotators among the G to M dwarf range in NGC 6475, their x-ray flux being too weak to have been detected. The existence of a significant number of additional low-mass cluster members with $\log L_x<29.0$ would then change the relatively constant $\langle \log L_x \rangle$ distribution seen in Table 7 into one in which $\langle \log L_x \rangle$ decreases from early G to late-K dwarfs, as in the Pleiades.[4] A deep *BVI* photometric survey of the NGC 6475 region would provide the means to recover any members which were not detected in x rays. Such complementary membership surveys not based on coronal activity levels are important in order to prevent the x-ray properties of the NGC 6475 cluster from being biased

[4]This is true, under the consideration that the cluster luminosity function would be increasing as a function of decreasing mass over this spectral range.

by the preferential detection of rapid rotators and binary systems.

4. CONCLUSION

Approximately 140 x-ray sources have been found in a 46 ks *ROSAT* PSPC observation of the ~220 Myr old open cluster NGC 6475. *BVI* CCD photometry of the cluster region has provided improved magnitudes and colors for the bright cluster members and identified more than 100 new candidate cluster members: ~50 late F–K0 candidates and ~70 additional fainter candidates in the K/M dwarf range. The x-ray observations have proven to be an efficient means of identifying low-mass cluster members in a low-latitude galactic cluster for which membership determination by other means (i.e., photometric and proper motion surveys) was not as practical due to the cluster's distance and contamination from field stars. Yet, some low-mass members with low rotational velocities and consequently weak x-ray emission levels are likely to have been missed in the present study.

Several high-mass members of NGC 6475 are found to be associated with x-ray sources; the detection rate appears to be consistent with the supposition that most such stars detected are binary systems with the x-ray emission arising from the low-mass companion. A more complete study of the binarity of NGC 6475 members however is necessary in order to better ascertain the frequency of binary systems among NGC 6475 stars. For those early type (<F5) members and likely members not detected in x rays, 3σ upper limits have been determined.

In addition to new candidate members of NGC 6475, at least two very soft x-ray sources have been identified. Neither of these appears to be associated with a cluster member, but might prove to be of interest if found to be associated with some unusual stellar system other than nearby stars. One x-ray source, diffuse in appearance, was observed and may be associated with a previously unknown, more distant open cluster.

A limited discussion of the x-ray properties of the members of NGC 6475 has been presented. Radial and rotational velocities have been obtained for a sample of the new optical candidates, generally confirming membership and the predominance of low $v \sin i$ values among solar-type stars. Additional follow-up spectroscopy is necessary however in order to provide more complete information on rotational velocities and binarity, and to confirm cluster membership for the current photometric members. With the present candidate members, the upper envelope of $\log L_x$ as a function of color (or mass) in NGC 6475 is similar to that seen in the Pleiades, with a factor of ~10 spread in x-ray luminosity among the low-mass members. The distribution of $\log(L_x/L_{bol})$ indicates that the saturation level for NGC 6475 stars is reached at a spectral type (or color) intermediate between that of the much younger IC 2602 cluster and the older Praesepe cluster, consistent with the expectations of the spindown of solar-type stars after their arrival on the main-sequence. Further investigation of the properties of the new candidate members identified here will enable a more extensive discussion of coronal activity among NGC 6475 stars and their relation to stars observed in both older and younger clusters.

R.A.S. was supported in part by the Lockheed Independent Research Program. This work is partially based on observations obtained at the European Southern Observatory, La Silla, Chile. Support for this research, including the CTIO observing program, has been provided by NASA Grant Nos. NAG5-2171 and NAGW-2698. C.P./S.R. acknowledge the helpful assistance of the CTIO and ESO personnel. Discussions with Sangeeta Mysore concerning the x-ray data and source list are also acknowledged.

APPENDIX A

Finding charts are provided for those x-ray sources in Tables 4 and 5 which are not associated with bright stars from the survey of Koelbloed (1959). (see Figs. 10–15) (Plates 43–48). Charts are approximately 3×3 arcmin, with north up and east to the left, and are extracted from *V*-band CCD frames. The circles are centered at the position of the x-ray detection and have a radius of ~30 arcsec. In addition to those stars listed in Tables 4 and 5, other stars in the field of the x-ray source are listed below in some cases. The stars listed in Tables 4 and 5 and in the notes below are marked in the accompanying charts; the individual offsets should be consulted for cases of multiple optical counterparts. Offsets in arcseconds are given in terms of (x-ray-optical) positions, as in Tables 4 and 5. Bright stars from the list of Koelbloed are identified for assistance if they fall within the field of view. Individual notes on the finding charts:

R3: C) GSC 7386.0531: $(V,V-I_C)=(12.54,0.44)$, offset $=(+7,+49)$, photometry nonmember.

R4: A) GSC 7386.0989*S* (southern comp.): $(V,V-I_C)$ $=(12.20,0.82)$, offset$=(+37,+40)$, Y candidate.

R11: B) GSC 7386.0553: $(V,B-V,V-I_C)=(11.41,1.30,1.35)$, offset$=(+12,+4)$, photometry nonmember.

R13: B) GSC 7386.0826: $(V,B-V,V-I_C)=(13.66,0.63,0.82)$, offset$=(+35,-24)$, photometry nonmember.
A possible nebulous object also lies at the x-ray position.

R34: B) GSC 7386.0711: $(V,V-I_C)=(11.66,0.38)$, offset $=(+22,-29)$, phot. nonmember.
C) $(V,V-I_C)=(13.13,0.77)$, offset$=(-12,+11)$, phot. nonmember.

R37: B) $(V,B-V,V-I_C)=(14.17,1.66,1.83)$, offset $=(-19,-1)$, phot. nonmember.

R55: C) $(V,B-V,V-I_C)=(15.05,0.73,0.92)$, offset $=(+1,+6)$, phot. nonmember.

R67: B) $(V,V-I_C)=(15.42,1.84)$, offset$=(+18,-45)$, Y? candidate.

R71: The bright star within circle is K79: $(V,B-V)$

=(9.01,0.16), offset=(−9,+20). While K79 is considered a cluster member, the small off-axis distance of this x-ray source would suggest the fainter photometry candidate is the optical counterpart.

R76: B) $(V,B-V,V-I_C)$=(15.13,1.05,1.20), offset =(−1,−2), phot. nonmember.
C) $(V,B-V,V-I_C)$=(14.51,2.17,2.58), offset =(+7,+7), phot. nonmember.
D) $(V,B-V,V-I_C)$=(14.55,1.97,2.28), offset =(+0,−13), phot. nonmember.

R87: B) GSC 7386.0150: $(V,B-V,V-I_C)$=(12.28,0.69,0.81), offset=(+45, +15), Y candidate. This star lies relatively far from the x-ray source and is not considered the primary optical counterpart candidate.

R98: B) GSC 7386.0900: $(V,B-V,V-I_C)$=(13.47,1.60,1.63), offset=(−9, −13), phot. nonmember.

R107: B) $(V,V-I_C)$=(16.15,3.72), offset=(−5,+10), phot. nonmember.
C) $(V,B-V,V-I_C)$=(14.22,1.82,2.04), offset =(−1,+15), phot. nonmember.
D) $(V,B-V,V-I_C)$=(13.86,0.81,0.29), offset =(−18,−17), phot. nonmember.
E) $(V,B-V,V-I_C)$=(13.64,1.82,1.98), offset =(+28,−2), phot. nonmember.

R111: C) $(V,B-V,V-I_C)$=(13.90,1.69,1.88), offset =(−5,−18), phot. nonmember.

R112: B) $(V,B-V,V-I_C)$=(13.73,1.57,1.70), offset =(+17,−9), phot. nonmember.
C) $(V,B-V,V-I_C)$=(13.81,2.08,2.43), offset =(+3,+15), phot. nonmember.

R117: B) $(V,V-I_C)$=(13.69,0.54), offset=(−30,+26), phot. nonmember.
C) $(V,B-V,V-I_C)$=(15.11,1.43,1.64), offset =(−30,−26), Y? candidate.
D) $(V,B-V,V-I_C)$=(15.23,1.38,1.50), offset =(−17,+28), Y? candidate.
E) $(V,V-I_C)$=(15.51,1.73), offset=(+26,+3), Y? candidate.

R122: C) $(V,V-I_C)$=(16.31,2.46), offset=(+1,−7), N? candidate.
D) $(V,V-I_C)$=(15.68,1.61), offset=(+7,+17), ? candidate.

R126: B) $(V,B-V,V-I_C)$=(13.12,0.60,0.71), offset =(−1,+6), phot. nonmember.
C) $(V,B-V,V-I_C)$=(13.81,1.44,1.56), offset =(+8,+24), phot. nonmember.

R131: D) $(V,B-V,V-I_C)$=(11.90,0.36,0.49), offset =(−37,−34), phot. nonmember.
E) $(V,B-V,V-I_C)$=(13.77,0.87,1.04), offset =(−25,+27), N? candidate.

R132: B) fainter companion to visual binary GSC 7386.1351*B*: $(V,B-V,V-I_C)$=(13.41,2.09,2.90), offset=(0,−2), phot. nonmember.

R133: B) GSC 7386.1575: $(V,B-V,V-I_C)$ =(12.55,0.44,0.57), offset=(+31, +4), phot. nonmember.
C) GSC 7386.1856: $(V,B-V,V-I_C)$=(11.70,2.01,2.40), offset=(−24, +2), phot. nonmember.

R134: As no CCD frame currently exists for this location, the finding chart for this source is based on a Palomar plate scan. The GSC star listed in Table 4 is identified, however it is not necessarily considered to be the likely optical counterpart to the x-ray source.

R136: B) GSC 7386.1073: $(V,V-I_C)$=(13.48,0.85), offset =(−1,−25), phot. nonmember.

R138: The arrow indicates an extended or nebulous object, possibly a galaxy, in the field.

R140: C) $(V,V-I_C)$=(15.13,1.60), offset=(+24,+16), Y? candidate.

APPENDIX B

In this Appendix we present radial and rotational velocity measures obtained for a sample of stars comprised of previous known Koelbloed members and new optical candidates from Table 4. Observations were obtained during 1994 April by S. Randich using the ESO 3.6 m telescope with a multi-order cassegrain echelle spectrograph ("CASPEC") [Pasquini & Gilliotte (1993) and references therein], employing a Tektronix 512^2 CCD, 31.6 l/mm grating, short camera, and red cross-disperser. Order 88 in the echelle format, wavelength range ~6410–6495 Å at a 2 pixel resolution of 0.35 Å, was chosen by C.P. for v_{rad} and $v \sin i$ analysis due to the presence of several moderately strong Ca and Fe absorption lines. Due to instrument flexure, individual flatfields and thorium–argon lamps were taken for each observation. After flatfielding, the spectra were wavelength calibrated using the ONEDSPEC package in IRAF along with the thorium–argon exposure associated with a given observation.

Radial and rotational velocities were derived in the same manner as for observations of IC 4665 stars (Prosser & Giampapa 1994) to which the reader is referred for details. The radial velocity standards used in this program were HD 126053, HD 136202, HD 154417, and HD 187691, using the CfA radial velocities given by Latham & Stefanik (1991). From comparison of the radial velocities derived for a given target star using different radial velocity standards, the accuracy of the v_{rad} measures is considered to be only ~1–2 km/s at best (for narrow-lined spectra) and is dependent on the star's rotational velocity ($v \sin i$). Very rapid rotators (i.e., K66, K67, K75) will have uncertainties of several km/s in their v_{rad} measure. For rotational velocity measures, the wavelength range 6410–6480 Å was used and a high signal-to-noise day sky spectrum was employed as a calibration template. In Table 8 we give a summary of the results for the NGC 6475 stars observed, including a membership flag based on the observed radial velocity, the Julian date of ob-

TABLE 8. ESO CASPEC radial and rotational velocities (1994 April 21–25 UT).

Star	V	B−V	V−I_C	v_{rad} (km/s)	$v \sin i$ (km/s)	Mem?	JD − 2449400.	Notes
K 66	10.46	0.48	0.57	−6	50:	Y	66.87472	
K 67	10.66	0.43	0.56	−12:	70:	Y	67.85944	= R56
K 75	10.58	0.43	0.54	−9:	88:	Y	67.88053	= R65
K 84	10.24	0.51	0.63	+32	<10	Y	67.81722	SB2 (PhB)
	–	–	–	−39	18:	Y	67.81722	
K 93	11.27	0.54	0.65	−1	<10	N?	67.90819	
R14	12.06	0.66	0.77	−16	<10	Y	65.77368	GSC7386.0359, SB2
	–	–	–	+21:	<10	?	65.77368	weak component
R15	12.28	0.71	0.98	+24	13:	N?	65.87197	GSC7386.0151, SB2?
R16A	11.69	0.72	0.81	−12	<10	Y	63.92416	GSC7386.0794, PhB
R27	12.12	0.68	0.75	−17	<10	Y	65.79616	GSC7386.0904
R39B	12.19	0.69	0.81	+20	14	N?	65.83921	GSC7386.0023
R64	11.96	0.73	0.80	−16	<10	Y	67.92586	GSC7386.0171, northern comp.
R66	12.78	0.78	0.87	−5	<10	?	66.75089	GSC7386.0462, SB2?
	–	–	–	+24	–	?	66.75089	weak component
R73	10.95	0.57	0.69	−10	16	Y	63.84400	GSC7386.0355, PhB
R79	11.92	0.76	0.82	−17	13	Y	64.83113	GSC7386.1293
R95	12.19	0.68	0.78	−14	<10	Y	65.81936	GSC7386.0275
R97	12.17	0.69	0.76	−15	<10	Y	65.85554	GSC7386.0040
R105	12.32	0.70	0.80	−16	<10	Y	65.88920	GSC7386.0672
R109	12.63	0.80	0.95	−13	<10	Y	65.92058	GSC7386.1799
R119A	12.92	0.81	0.99	+25:	≤10	?	66.79812	GSC7386.1689, SB2
	–	–	–	−9:	≤10	?	66.79812	
R126A	11.45	0.56	0.68	−14	<10	Y	63.89998	GSC7386.1828
R127A	11.95	0.64	0.78	−15	<10	Y	64.84921	GSC7386.1353

servation, and additional notes. Of the 16 new optical candidates in Table 8, at least 12 are seen to have v_{rad} measures consistent with the approximate mean cluster velocity of ~ -15 km/s (Gieseking 1985; Abt *et al.* 1970), further confirming membership for these candidates identified from the x-ray survey. Two double-line spectroscopic binaries have been identified (K84 and R119A), while R14 and R66 appear to have a weak secondary component in their spectra and R15 exhibits a nonsymmetric cross-correlation profile suggestive of binarity. Among G-type stars ($B-V>0.6$), most stars have rotational velocities at or below the $v \sin i = 10$ km/s spectroscopic limit, consistent with the concept of rotational spin-down on the main sequence for a cluster of this age.

REFERENCES

Abt, H. A. 1975, PASP, 87, 417
Abt, H. A., Levy, S. G., Baylor, L. A., Hayward, R. R., Jewsbury, C. P., & Snell, C. M. 1970, ApJ, 159, 919
Bessell, M. S., & Weis, E. W. 1987, PASP, 99, 642
Bohlin, R. C., Savage, B. D., & Drake, J. F. 1978, ApJ, 224, 132
Caillault, J.-P., Gagné, M., & Stauffer, J. R. 1994, ApJ, 432, 386
Constantine, S. M., Harris, B. J., & Nikoloff, I. 1969, Proc. ASA 1, 207
Engberg, M. 1983, A&AS, 54, 203
Feigelson, E. D., & Nelson, P. I. 1985, ApJ, 293, 192
Fleming, T. A., Giampapa, M. S., Schmitt, J. H. M. M., & Bookbinder, J. A. 1993, ApJ, 410, 387
Gieseking, F. 1985, A&AS, 61, 75
Hoag, A. A., Johnson, H. L., Iriatre, B., Mitchell, R. I., Hallam, K. L., & Sharpless, S. 1961, Pub. U.S. Naval Obs. 17, 343
Jeffries, R., & James, D. J. 1994a, private communication
Jeffries, R., *et al.* 1994b, in The Eighth Cambridge Workshop on Cool Stars, Stellar Systems, and The Sun, ASP Conf. Ser. Vol. 64, edited by J.-P. Caillault, p. 101
Koelbloed, D. 1959, Bull. Astr. Inst. Netherlands, 14, 265
Kron, G., Gascoigne, S., & White, H. 1957, AJ, 62, 205
Landolt, A. 1992, AJ, 104, 340
Latham, D. W., & Stefanik, R. P. 1991, in Reports on Astronomy, IAU Transactions XXIB (Kluwer. Dordrecht), p. 269 (CfA preprint No. 3316)
LaValley, M., Isobe, T., & Feigelson, E. D. 1992, BAAS, 24, 839
Leung, K. C., & Schneider, D. P. 1975, ApJ, 201, 792
Lodén, L. O. 1984, A&AS, 58, 595
Mermilliod, J. C. 1981, A&A, 97, 235
Mermilliod, J. C., Mayor, M., Andersen, J., Nordström, B., Lindgren, H., & Duquennoy, A. 1989, A&AS, 79, 11
Meynet, G., Mermilliod, J.-C., & Maeder, A. 1993, A&AS, 98, 477
Pallavicini, R. 1989, A&AR, 1, 177
Pasquini, L., & Gilliotte, A. 1993, The ESO Messenger, 71, 54
Patten, B. M., & Simon, T. 1993, ApJ, 415, 123

Pfeffermann, E., *et al.* 1986, Proc SPIE, 733, 519
Prosser, C. F., & Giampapa, M. 1994, AJ, 108, 964
Pye, J. P., Hodgkin, S. T., Stern, R. A., & Stauffer, J. R. 1994, MNRAS, 266, 798
Randich, S., & Schmitt, J. H. M. M. 1995, A&A, 298, 115
Randich, S., Schmitt, J. H. M. M., Prosser, C., & Stauffer, J. R. 1995, A&A (in press)
Schild, R. E. 1983, PASP, 95, 1021
Snowden, M. S. 1976a, PASP, 88, 171
Snowden, M. S. 1976b, Centre Données Stellaires, Inf. Bull. 10, 30
Stauffer, J. R. 1982, AJ, 87, 899
Stauffer, J. R., Caillault, J.-P., Gagné, M., Prosser, C. F., & Hartmann, L. W. 1994, ApJS, 91, 625
Stern, R. A., Schmitt, J. H. M. M., & Kahabka, P. T. 1995, ApJ (in press)
Stern, R. A., Schmitt, J. H. M. M., Pye, J. P., Hodgkin, S. T., Stauffer, J. R., & Simon, T. 1994, ApJ, 427, 808
Stern, R. A., Schmitt, J. H. M. M., Rosso, C., Pye, J. P., Hodgkin, S. T., & Stauffer, J. R. 1992, ApJ, 399, L159
Stetson, P. B. 1987, PASP, 99, 191
Swenson, F. J., Faulkner, J., Rogers, F. J., & Iglesias, C. A. 1994, ApJ, 425, 286
Trümper, J. 1992, QJRAS, 33, 165